Multi-Sensor InSAR Railway Structure Monitoring:

Towards Generating Product-Level Deformation

[PROJECT ID. 95473]

2025 DRAGON 6 SYMPOSIUM

14-18 JULY 2025







ID. 95473

PROJECT TITLE: MULTI-SENSOR INSAR RAILWAY STRUCTURE MONITORING: TOWARDS GENERATING PRODUCT-LEVEL DEFORMATION

PRINCIPAL INVESTIGATORS: MENGSHI YANG, RAMON HANSSEN

CO-AUTHORS: WIETSKE BROUWER, YANGWEI YU, HAO WU, LINA HAGENAH, YUQING WANG

PRESENTED BY: RAMON HANSSEN

Project Background



Rail infrastructure of the Netherlands



China-Laos Railway







The structural health of the railway tracks
The stability of the surrounding area → **essential**













Earlier work

Chang, L., Dollevoet, R.P. and Hanssen, R.F., 2016. Nationwide railway monitoring using satellite SAR interferometry. *IEEE Journal of Selected Topics in Applied Earth Observations and Remote Sensing*, *10*(2), pp.596-604.

Chang, L. and Hanssen, R.F., 2015. Detection of permafrost sensitivity of the Qinghai–Tibet railway using satellite radar interferometry. *International journal of remote sensing*, *36*(3), pp.691-700.

Hanssen, R., Chang, L. and Dollevoet, R., 2015. Automatic railway instability detection using satellite SAR interferometry. In *Mapping Urban Areas from Space*.

Chang, L., Dollevoet, R.P.B.J. and Hanssen, R.F., 2014. Railway infrastructure monitoring using satellite radar data. *Int. J. Railw. Technol*, *3*(2), pp.79-91.

Chang, L., Sakpal, N.P., Elberink, S.O. and Wang, H., 2020. Railway infrastructure classification and instability identification using Sentinel-1 SAR and laser scanning data. *Sensors*, *20*(24), p.7108.

Chang, L., Dollevoet, R.P. and Hanssen, R.F., 2018. Monitoring line-infrastructure with multisensor SAR interferometry: Products and performance assessment metrics. *IEEE journal of selected topics in applied earth observations and remote sensing*, *11*(5), pp.1593-1605.

Hu, F., Leijen, F.J.V., Chang, L., Wu, J. and Hanssen, R.F., 2019. Monitoring deformation along railway systems combining multi-temporal InSAR and LiDAR data. *Remote sensing*, *11*(19), p.2298.

Chang, L., Hanssen, R.F. and Dollevoet, R.P.B.J., 2016. Detection of railway infrastructure settlement using satellite SAR interferometry. In *Proceedings of the Second International Conference on Railway Technology: Research, Development and Maintenance* (Vol. 110). Civil-Comp Press.

Wang, H., Chang, L. and Markine, V., 2018. Structural health monitoring of railway transition zones using satellite radar data. *Sensors*, *18*(2), p.413.

van Leijen, F., Chang, L. and Hanssen, R., 2016. Systematic Anomaly Detection for Rails and Embankments using Satellite Radar Interferometry. In *Dragon 3 Final Results Symposium*.

Hu, F., Van Leijen, F.J., Chang, L., Wu, J. and Hanssen, R.F., 2021. Combined detection of surface changes and deformation anomalies using amplitude-augmented recursive inSAR time series. *IEEE transactions on geoscience and remote sensing*, *60*, pp.1-16.

Yang, M., López-Dekker, P., Dheenathayalan, P., Biljecki, F., Liao, M. and Hanssen, R.F., 2019. Linking persistent scatterers to the built environment using ray tracing on urban models. *IEEE Transactions on Geoscience and Remote Sensing*, *57*(8), pp.5764-5776.

Qin, X., Liao, M., Zhang, L. and Yang, M., 2017. Structural health and stability assessment of high-speed railways via thermal dilation mapping with time-series InSAR analysis. *IEEE Journal of Selected Topics in Applied Earth Observations and Remote Sensing*, *10*(6), pp.2999-3010.

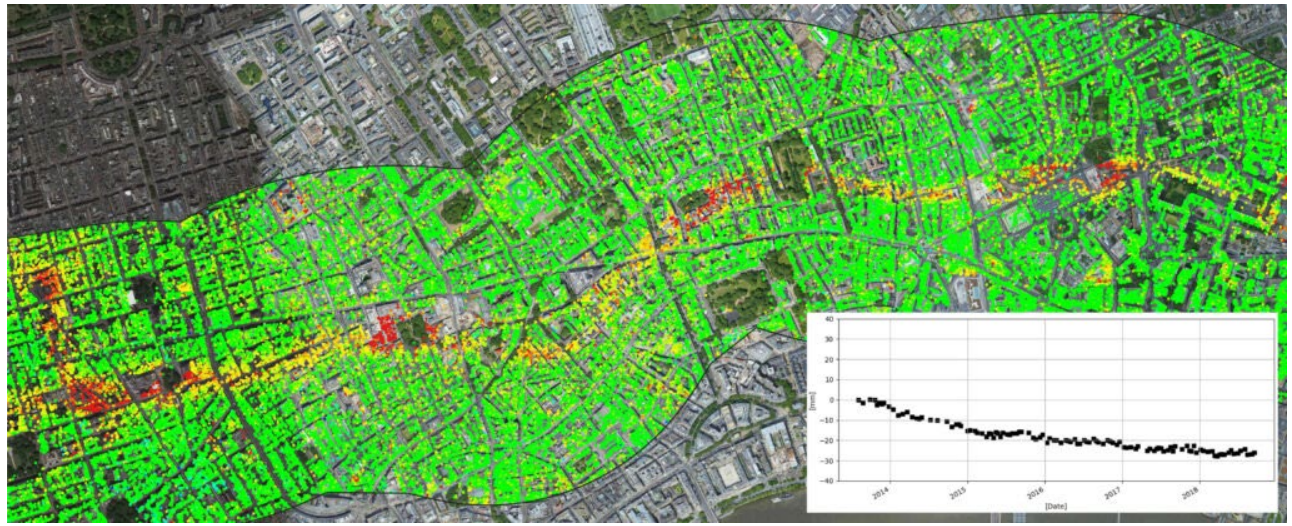
Qin, X., Liao, M., Yang, M. and Zhang, L., 2017. Monitoring structure health of urban bridges with advanced multi-temporal InSAR analysis. *Annals of GIS*, *23*(4), pp.293-302.

Yang, M., Liao, M., Chang, L. and Hanssen, R.F., 2023. 城市场景时序 InSAR 形变解译: 问题分析与研究进展. *Wuhan Daxue Xuebao (Xinxi Kexue Ban)/Geomatics and Information Science of Wuhan University*, *48*(10), pp.1643-1660.

Wang, R., Yang, M., Dong, J. and Liao, M., 2022. Investigating deformation along metro lines in coastal cities considering different structures with InSAR and SBM analyses. *International Journal of Applied Earth Observation and Geoinformation*, *115*, p.103099.

Project Background

InSAR



- Low cost and fast solution
- Periodic monitoring
- Wide-scale high resolution surface displacements

Drone



affected by weather conditions

Leveling & GNSS



manpower & resources

Laser And Lidar



Point-based & resources

Distributed fiber

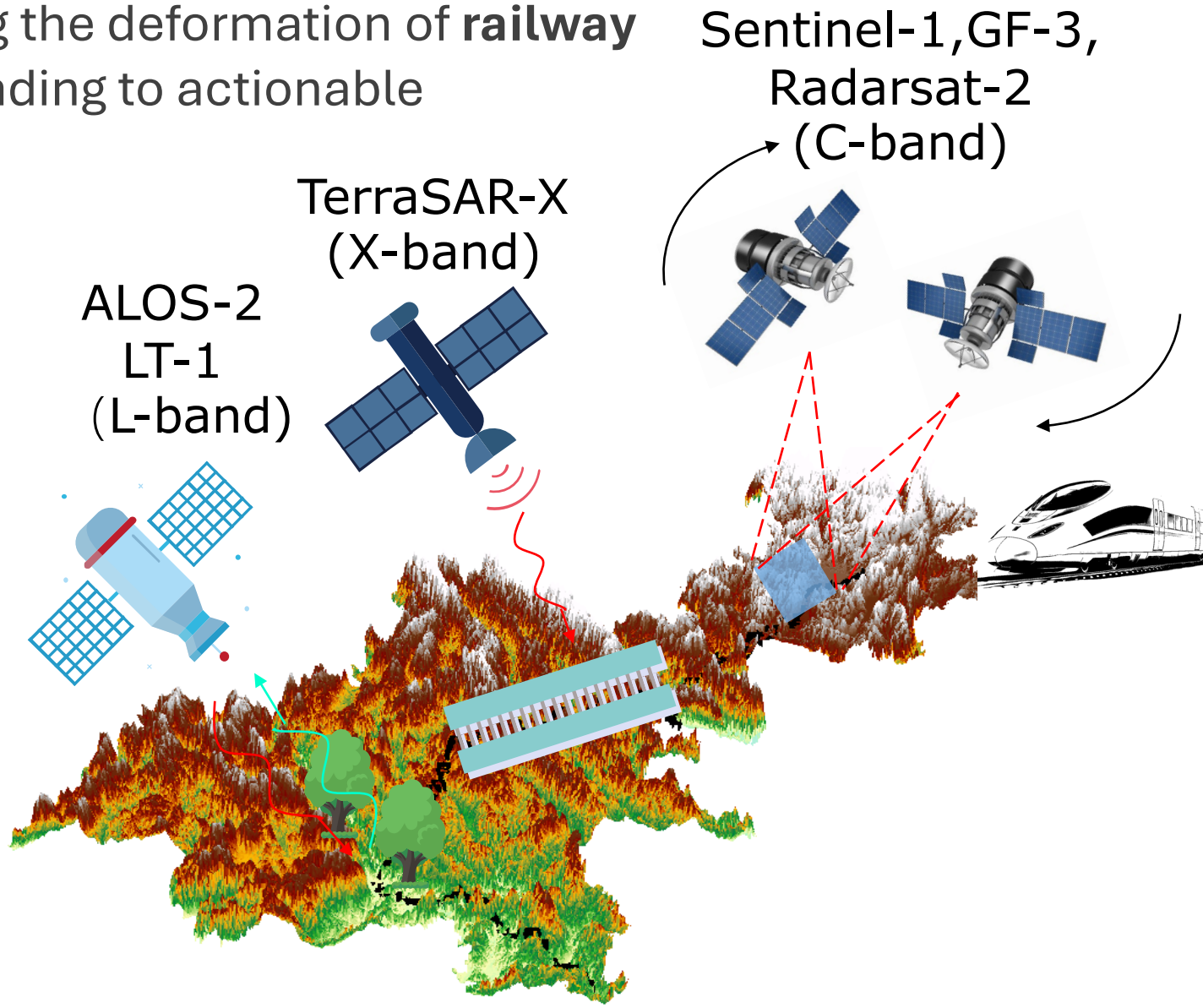


Lack of stability

Project objective

Further developing **InSAR** to monitoring the deformation of **railway structures and surrounding areas,** leading to actionable information:

- **InSAR deformation estimation model for linear infrastructure**
- **InSAR-based metrics to detect anomalous displacement signals**
- **InSAR-based operational products for railway asset management**

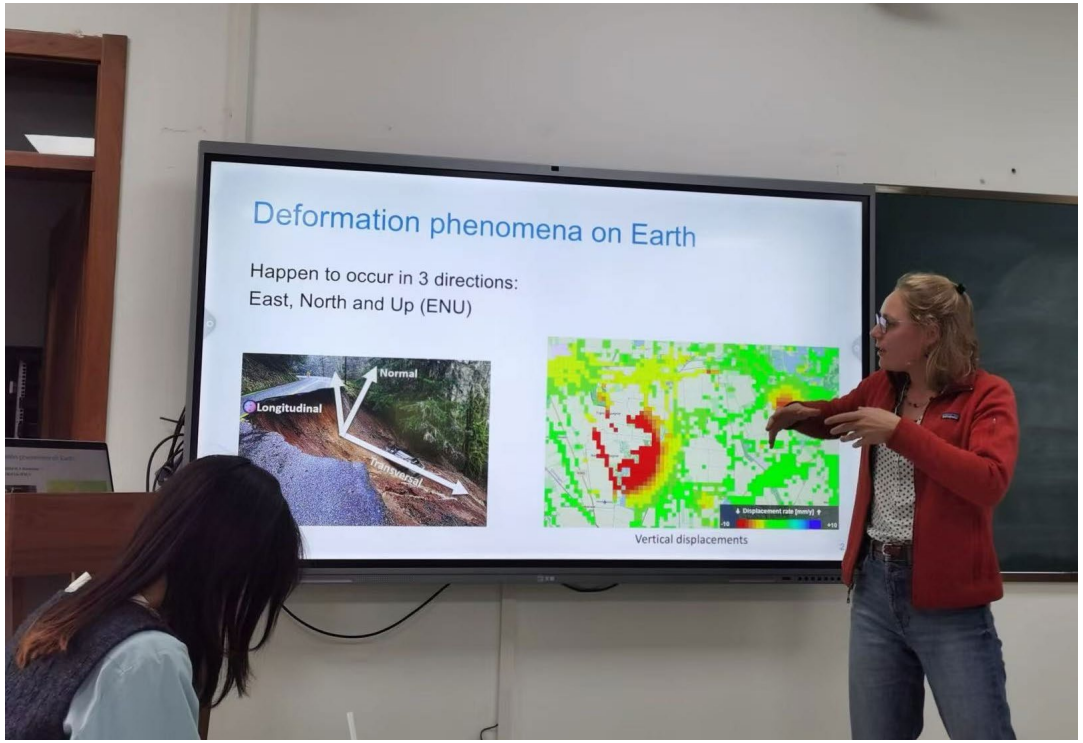


Academic Exchanges

- Research Collaboration & Academic Visit (2024.11)

•Ms. Wietske Brouwer, a PhD candidate from Delft University of Technology (TUD), the Netherlands, conducted a one-month academic visit and exchange at Yunnan University. During her stay, she engaged in joint research on short-baseline InSAR inversion methodologies. This collaboration further strengthened the amicable cooperative ties between young scientists from China and the Netherlands.



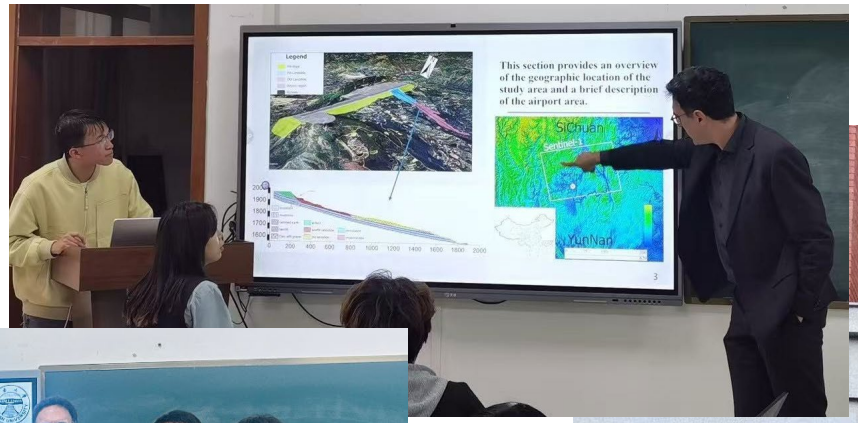


Academic Exchanges

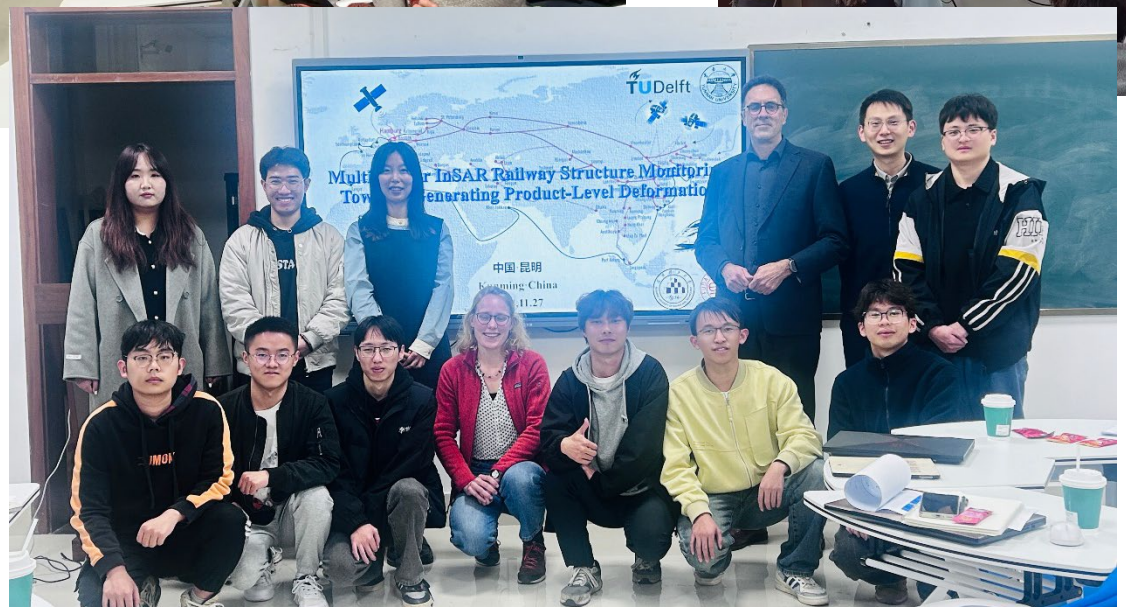
- Research Collaboration & Academic Visit (2024.12)

•Ramon Hanssen, the Dutch Principal Investigator (PI) of this project and a member of the Radar Remote Sensing group at TUD, was invited to visit Yunnan University.
•Both sides held in-depth discussions on the research outcomes achieved under the project.











Academic Exchanges

- Research Collaboration & Academic Visit (2025.7)

  - **Young scientists from the project convened a learning and exchange symposium in Kunming, Yunnan.**







  - **The event brought together early-career researchers from four participating institutions: TUD, YNU, KUST, and SWFU.**

Academic Exchanges

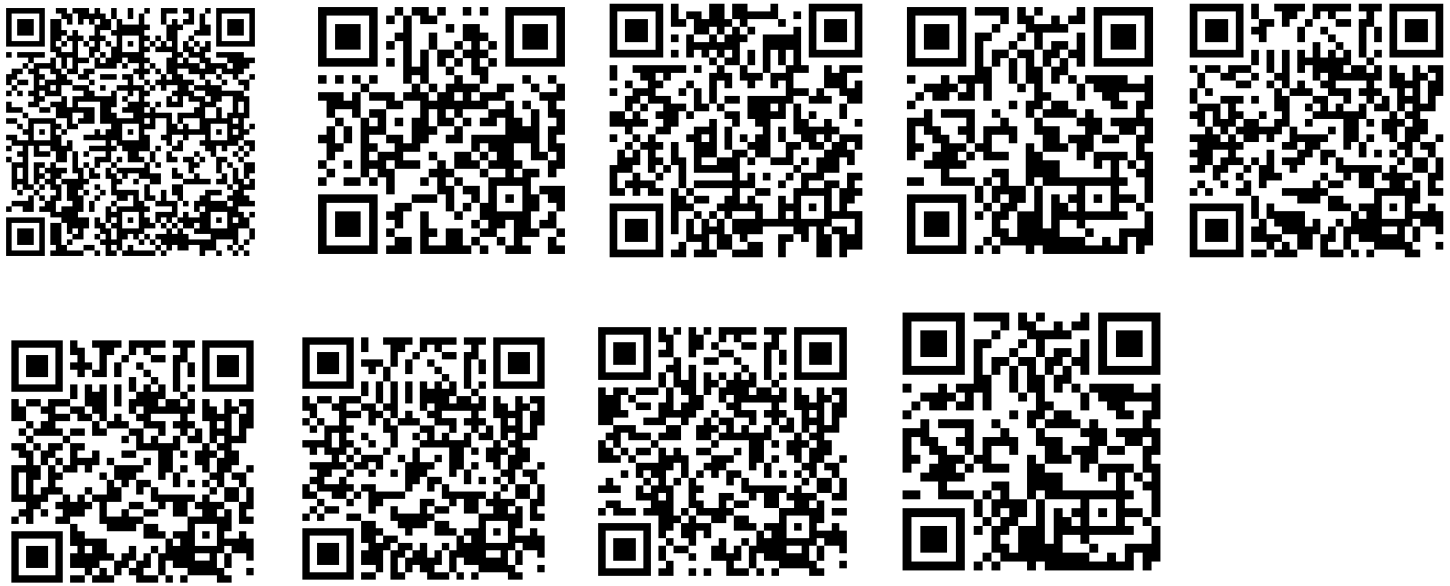
- Team Members' Conference Contributions (CH)

Time	Location	Conference	title	member
2024.5.13-2024.5.17	Changsha, China	ISPRS TC I Symposium on Intelligent Sensing and Remote Sensing Application	Revealing Urban Deformation Patterns through InSAR Time Series Analysis with TCN and Transfer Learning（Best Paper）	Mengshi Yang(PI)
2025.5.17-2024.5.23	Xi'an, China	大地测量与导航2024综合学术年会暨大地测量学科发展研讨会	城市场景InSAR形变解译：来自散射机制和机器学习视角	Mengshi Yang(PI)
2024.6.14-2024.6.16	Wuhan, China	第一届雷达干涉测量学术研讨会	城市场景InSAR形变解译 星载InSAR非侵入式建筑稳定性评估方法研究 面向城市场景的异轨多源InSAR点云融合（优秀快播报告） 基于FC-AE自监督学习的InSAR时序形变重建	Mengshi Yang Weibin Huang(YS) Zhuo Yang(YS) Hang Yu(YS)
2024.7.11-2024.7.13	Kunming, China	第二届城市可持续发展研讨会	星载InSAR视角下城市基础设施健康监测	Mengshi Yang(PI)
2024.10.22-2024.10.24	Suzhou, China	The 8th Digital Belt and Road Conference (DBAR2024)	Building Stability Assessment through Satellite SAR Interferometry: Contributions toward SDG11	Mengshi Yang(PI)
2024.11.22.-2024.11.24	Zhuhai, China	IEEE International Conference on Signal, Information and Data Processing 2024	Influence of multipath scattering on InSAR scatterers in Urban for deformation monitoring Evaluating the influence of ETAD product for PSI estimation	Mengshi Yang(PI) Hao Wu(YS)
2024.12.4-2024.12.8	Hongkong, China	The 2nd Youth Innovation Forum on Digital Earth	Deep Learning-Based Reconstruction and Classification of InSAR Displacement Time Series for Urban Monitoring	Mengshi Yang(PI)
2025.5.20-2025.5.25	Suzhou, China	□□□□□□□□□□□□□□	□□ InSAR□□□□□□□□□□□□□□□□	Mengshi Yang(PI)

Academic Exchanges (European)

Year	Title	Authors	Type	Venue
2023	A Treatise on InSAR Geometry and 3-D Displacement Estimation	W. S. Brouwer, R. F. Hanssen	Journal article	IEEE Transactions on Geoscience and Remote Sensing
2023	Bridging Loss-of-Lock in InSAR Time Series of Distributed Scatterers	P. Conroy, S. A. N. van Diepen, F. J. van Leijen, R. F. Hanssen	Journal article	IEEE Transactions on Geoscience and Remote Sensing
2023	Stochastic Modeling for InSAR Arcs	W. S. Brouwer, R. F. Hanssen	Preprint / Abstract	EGU General Assembly
2024	Estimating Three-Dimensional Displacements with InSAR: the Strapdown Approach	W. S. Brouwer, R. F. Hanssen	Journal article	Journal of Geodesy
2024	Constrained Recursive Parameter Estimation for InSAR ARCS	Y. Wang, W. S. Brouwer, F. J. van Leijen, R. F. Hanssen	Conference paper / Oral	IEEE IGARSS 2024
2024	On the Treatment of the Reference Image for InSAR Parameter Estimation for Point Scatterers	W. S. Brouwer, R. F. Hanssen	Conference poster	IEEE IGARSS 2024
2024	First Wide-Area Dutch Peatland Subsidence Estimates Based on InSAR	P. Conroy, Y. Lumban-Gaol, S. van Diepen, F. J. van Leijen, R. F. Hanssen	Conference paper / Oral	IEEE IGARSS 2024
2024	SARXarray and STMtools: Open-Source Python Libraries for InSAR Data Processing and Analysis	O. Ku, F. Alidoost, P. Chandramouli, T. van Lankveld, F. Nattino, M. Grootes, F. J. van Leijen, R. F. Hanssen	Conference paper / Oral	IEEE IGARSS 2024
2024	Estimating Three-Dimensional Displacements with InSAR: the Strapdown Approach	W. S. Brouwer, R. F. Hanssen	Journal article	Journal of Geodesy

QR codes to these publications



Overview of Chinese YSs research

1. Improving PSI Estimation with Sentinel-1 ETAD: Insights into Phase Stability, Deformation Rates, and PS Localization

2. Railway Deformation Zone Mapping via InSAR Phase Gradient Stacking: Chinese Section of China-Laos Railway

Overview of Chinese YSs research

Overview of Chinese YSs research (when applicable)

Extended Time Annotation Products

1. Improving PSI Estimation with Sentinel-1 ETAD: Insights into Phase Stability, Deformation Rates, and PS Localization

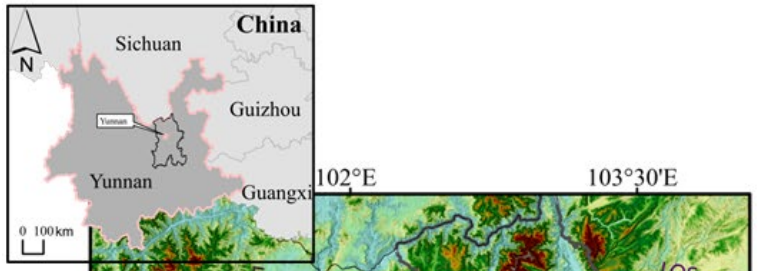
- **This study proposes a PSI processing strategy that integrates multiple correction layers from Sentinel-1 ETAD,** including both phase delays (e.g., tropospheric, ionospheric, solid Earth tides) and precise timing refinements in azimuth and range to improve imaging geometry.
- **A comprehensive evaluation** compares this approach with three benchmarks—(i) no correction, (ii) GACOS-based correction, and (iii) spatiotemporal filtering—demonstrating ETAD's effectiveness in enhancing interferogram quality, deformation accuracy, time series stability, and PS geolocation.

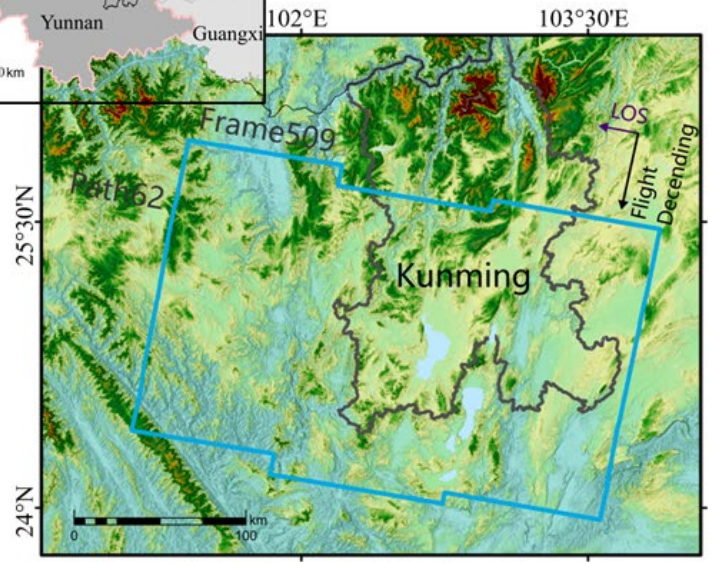
ETAD products

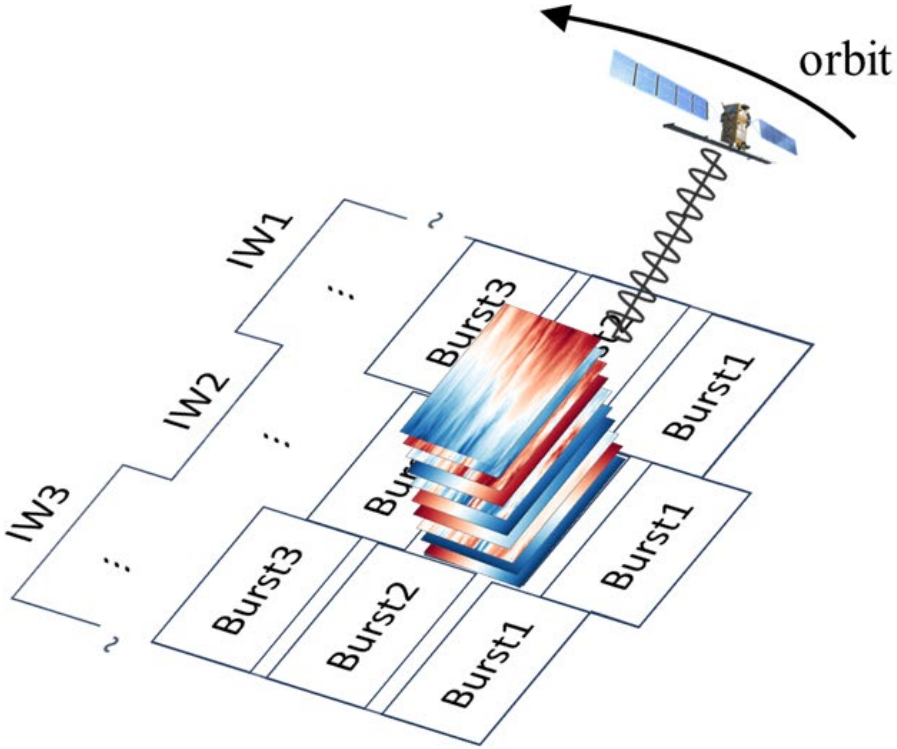
General	
Projection	Range-azimuth timing corrections grid
Spatial resolution	200m
Temporal resolution	12 days
ETAD product format	SAFE
Correct layer	
Tropospheric delay in range	Integrated NWM for delay correction.
Ionospheric delay in range	Computed from GNSS-based TEC maps.
Solid Earth tidal displacements	Corrected using Sun/Moon positions, ITRF model, and ephemeris.
Bistatic azimuth shifts	Corrected via inverse and precise grid corrections.
Doppler-induced range shifts	Corrected using Doppler center frequency and FM rate.
FM-rate mismatch azimuth shifts	Corrected using Doppler center, SAR processor FM rate, and geometry-based FM rate.

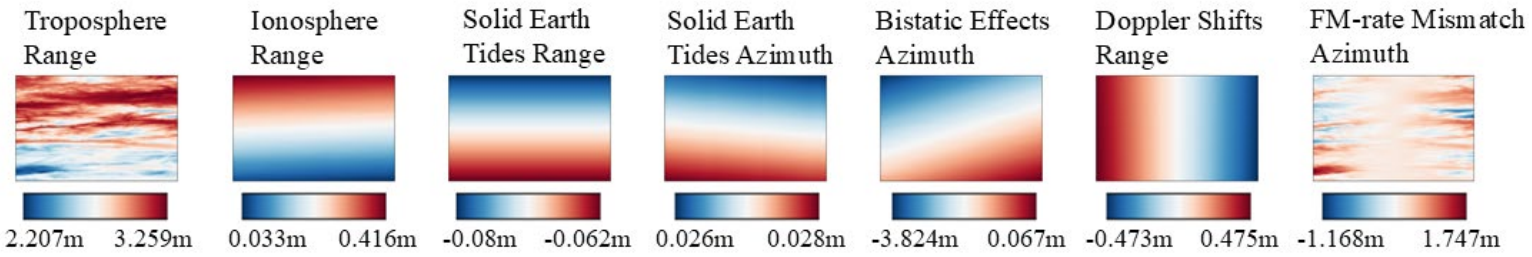
Improving PSI Estimation with Sentinel-1 ETAD: Insights into Phase Stability, Deformation Rates, and PS Localization

ETAD products









- The scope of the ETAD dataset is consistent with S-1
- Store in Burst format
- Contains 6 correction layers of independent data

Comparison of actual delays with official data:

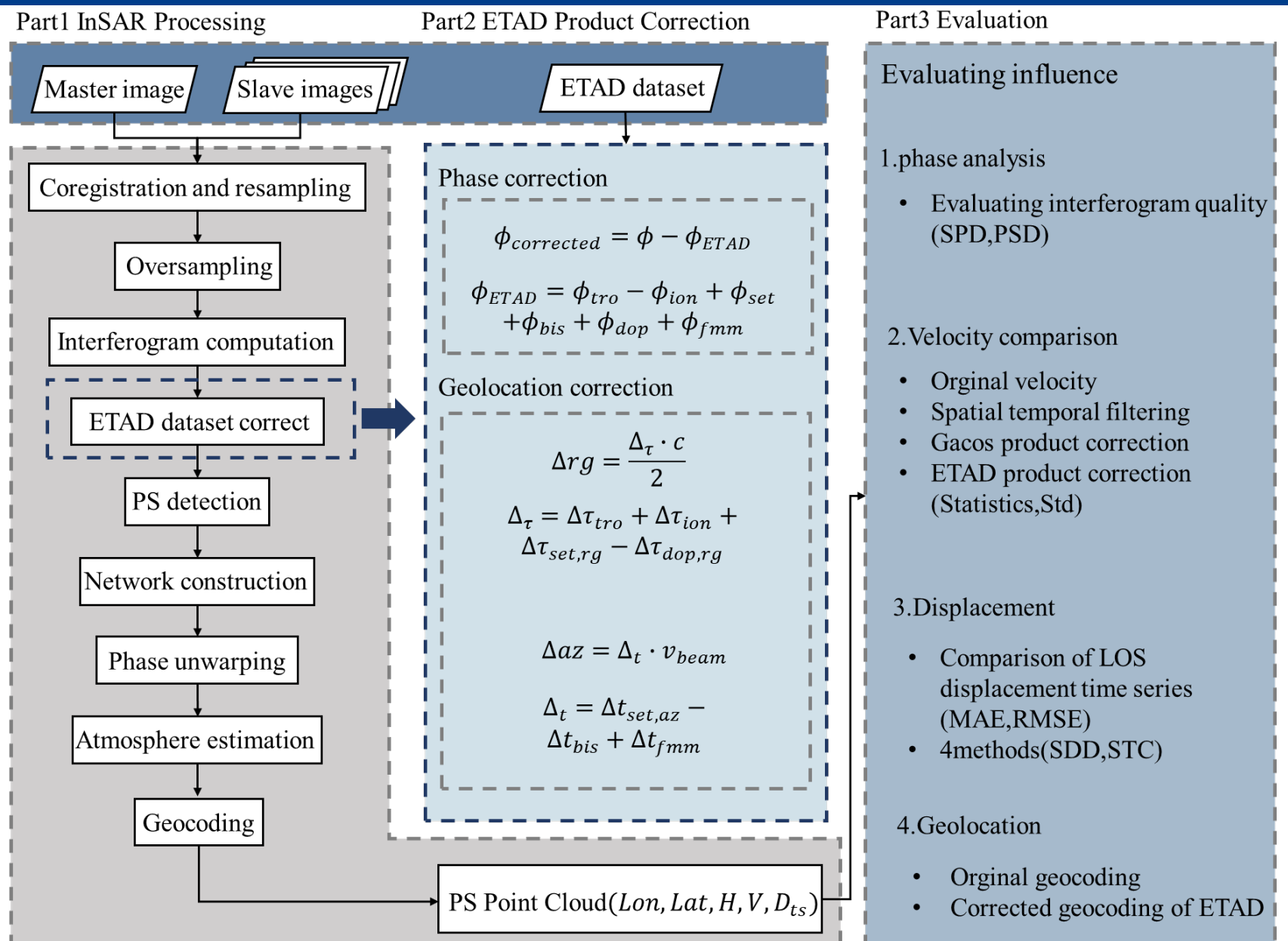
Correct layer	Calculated range(m)	ESA Document Scope(m)
TRO_{rg}	2.207 - 3.259	0.5-4.5
ION_{rg}	0.033 – 0.416	0-2
SET_{rg}	-0.080 - -0.062	-0.2 - 0.2
SET_{az}	0.026 – 0.028	-0.2 - 0.2
BIS_{az}	-3.824 – 0.067	-5 – 0.5
DOP_{rg}	-0.473 – 0.475	-0.5 – 0.5
FMM_{az}	-1.168 – 1.747	<6

Methodology

Part1
Incorporating ETAD data into the regular PSI processing workflow

Part2
Apply ETAD's correction principle

Part3
Evaluating the impact of ETAD on PSI (four aspects)
- Interferogram
- Velocity
- Deformation
- Geolocation



Methodology

$$l_{sr} = c\frac{\tau_{sr}}{2}$$

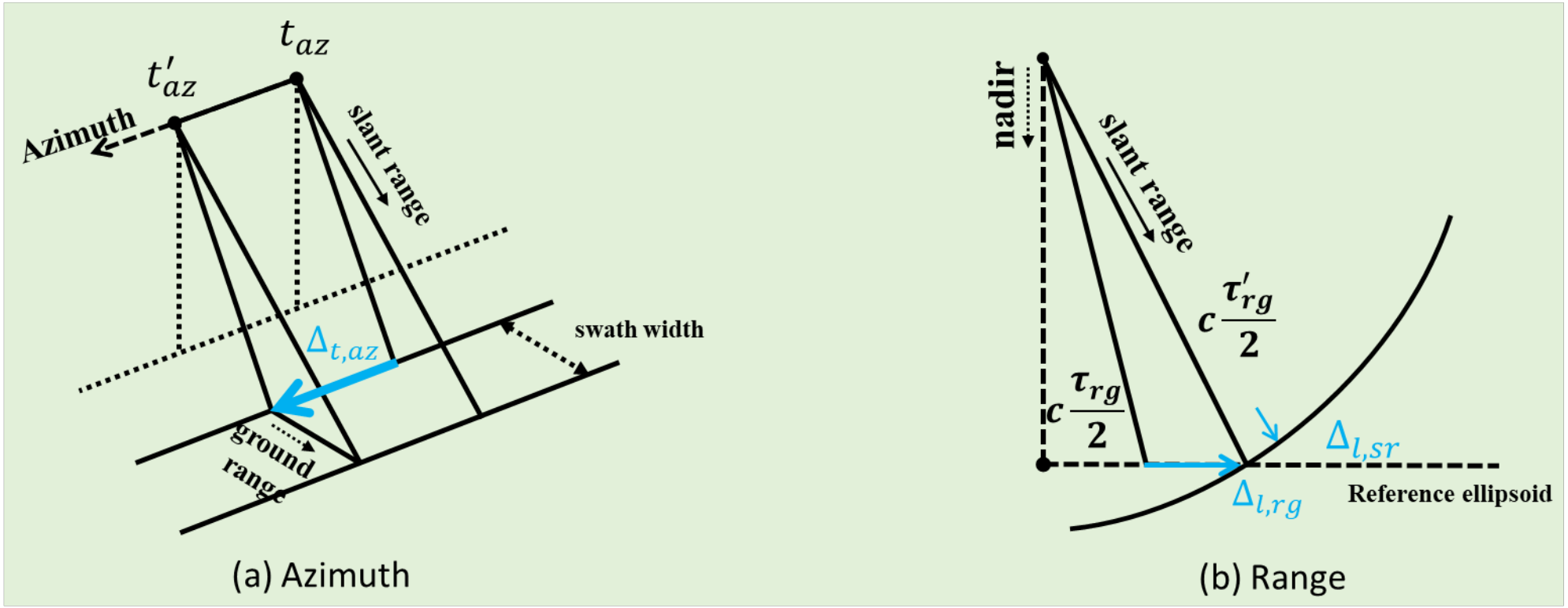
Azimuth:

$$\Delta l_{az} = v_g(t'_{az} - t_{az})$$

$$\Delta l_{sr} = c\,\frac{\tau'_{rg} - \tau_{rg}}{2}\, and, \Delta l_{gr} = \frac{\Delta l_{sr}}{sin\theta}.$$

v_g: speed of the satellite on the ground

θ:local incident angle



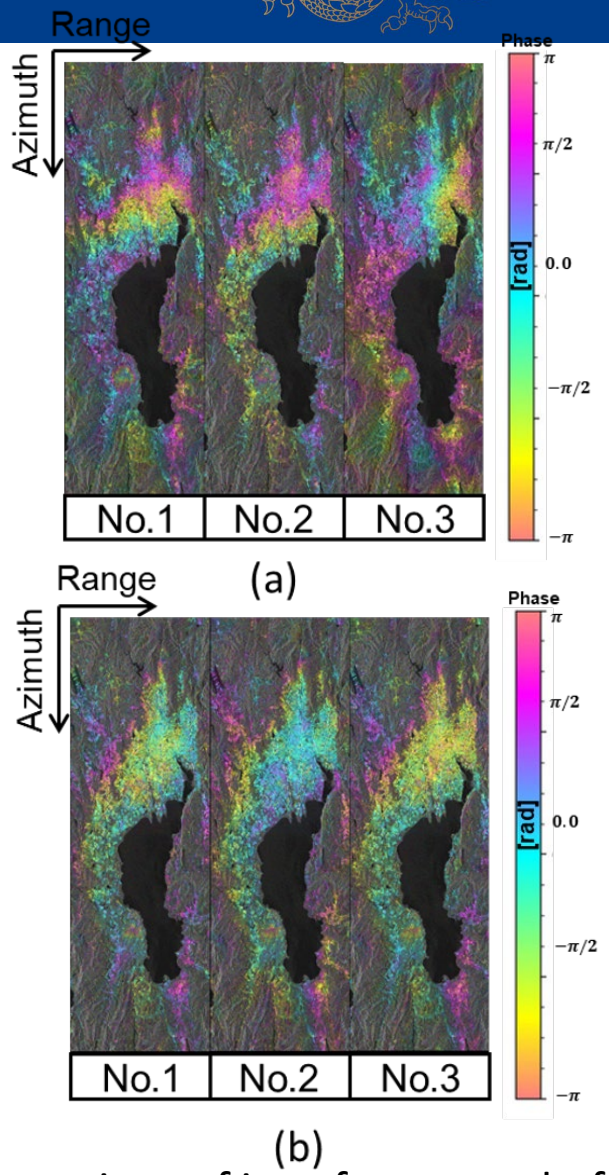
Results-Interferogram

Comparison of interference patterns before and after correction

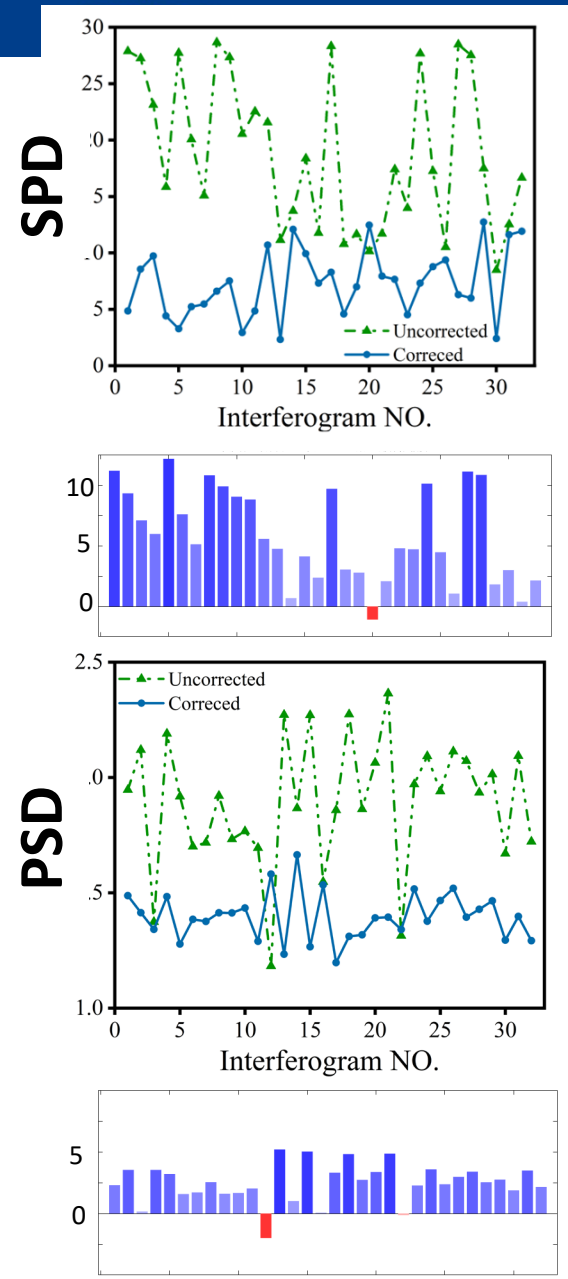
- the Sum of Phase Differences (SPD) is reduced by 61% compared to the uncorrected interferograms,
- the Phase Standard Deviation(PSD) is reduced by 40%

Comparison of interferogram quality before and after ETAD phase correction using SPD and PSD metrics:

Interferogram Type	SPD	PSD
Original interferograms	18.94	1.875
Corrected interferograms	7.43	1.392
Relative improvement (%)	60.77%	40.30%

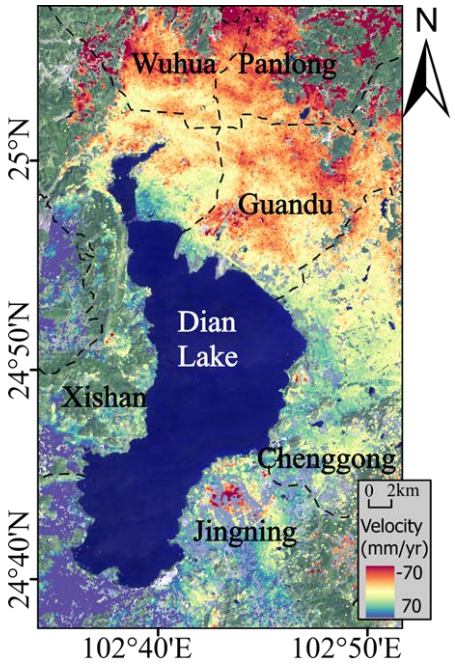


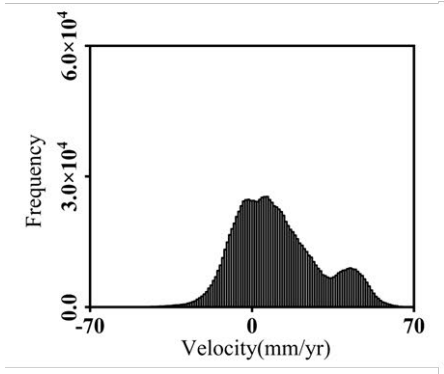
Comparison of interferograms before and after ETAD correction



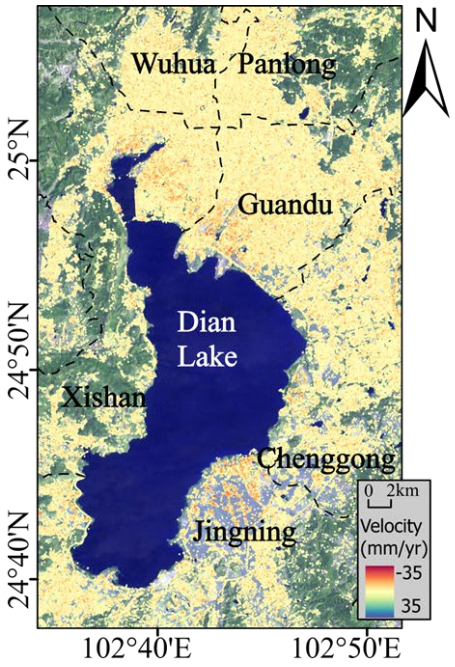
Results-velocity

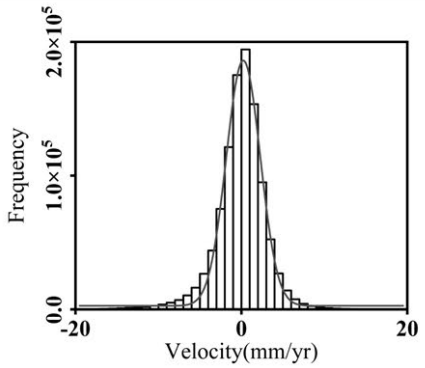
Orginal



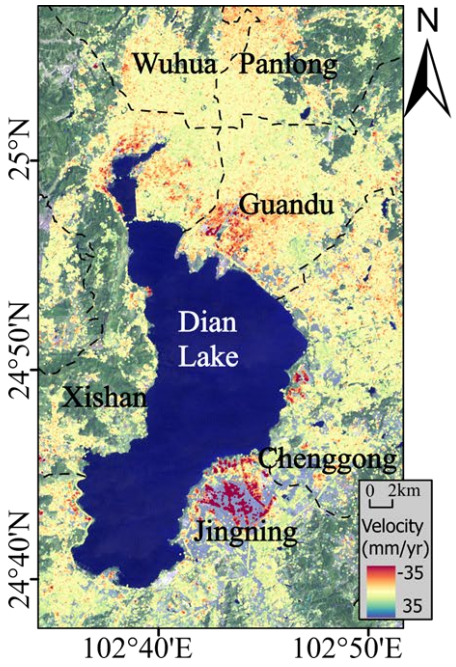


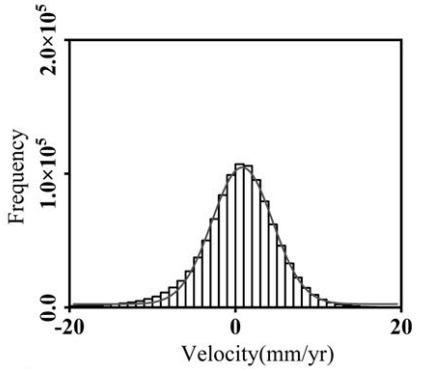
TSF



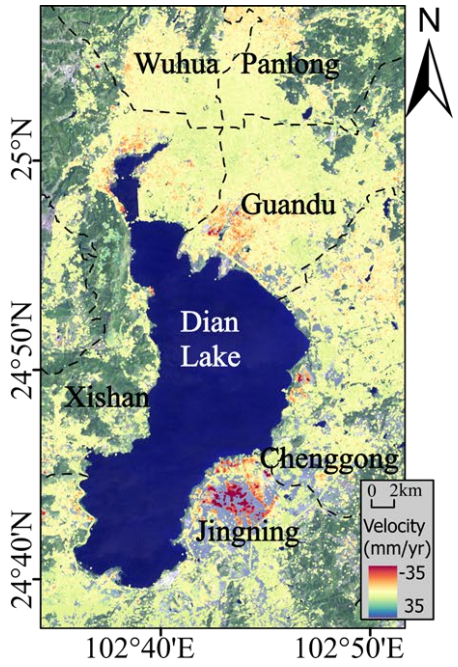


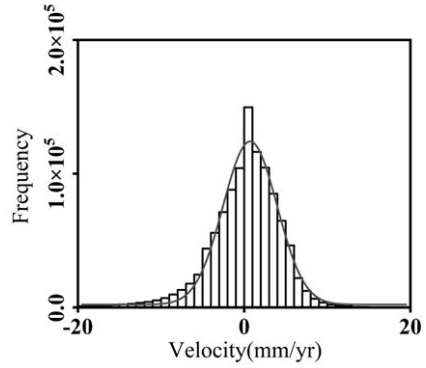
GACOS





ETAD



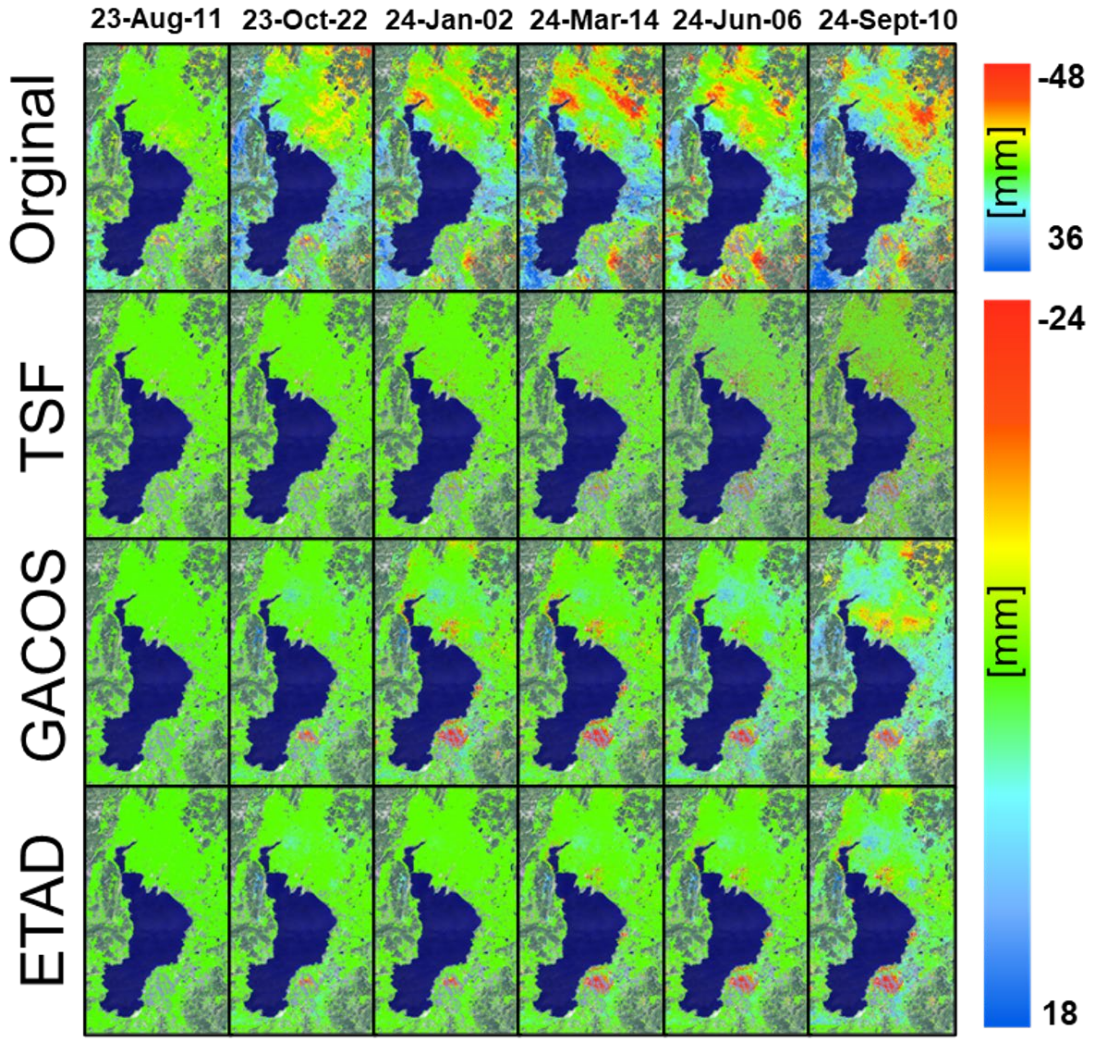


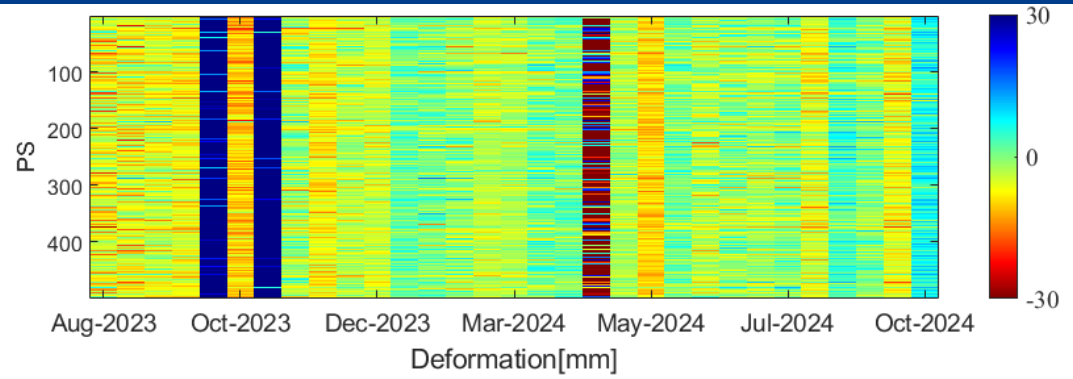
STD:

Original: 18.64mm/yr
TSF:2.82mm/yr
GACOS:6.34mm/yr
ETAD:5,26mm/yr

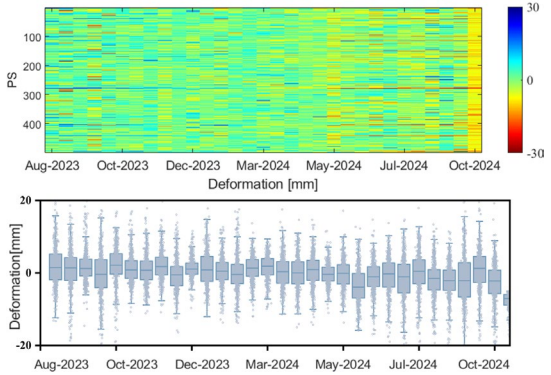
- TSF has excessive filtering (reducing 85%)
- GACOS does not filter out errors cleanly (reducing 66%)
- ETAD has better rate results (reducing 72%)

Results-time series

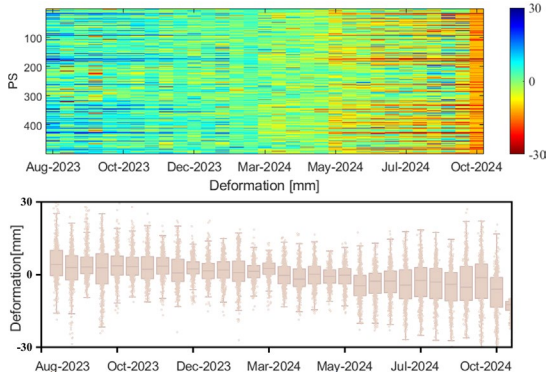




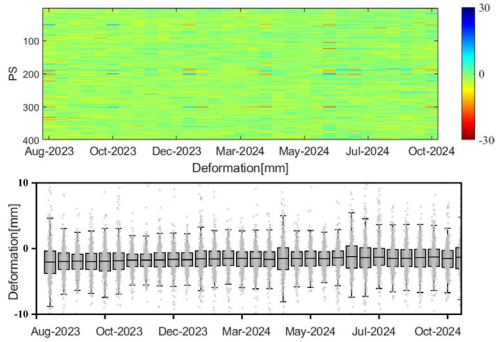
(a)



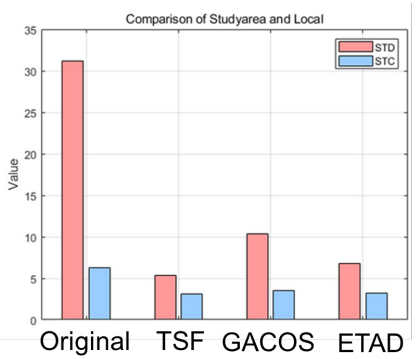
(b)



(c)



(d)



Results-geolocation

$Range\ offset[m]$:

Mean： 5.6

Std dev： 0.5

$Azimuth\ offset[m]$:

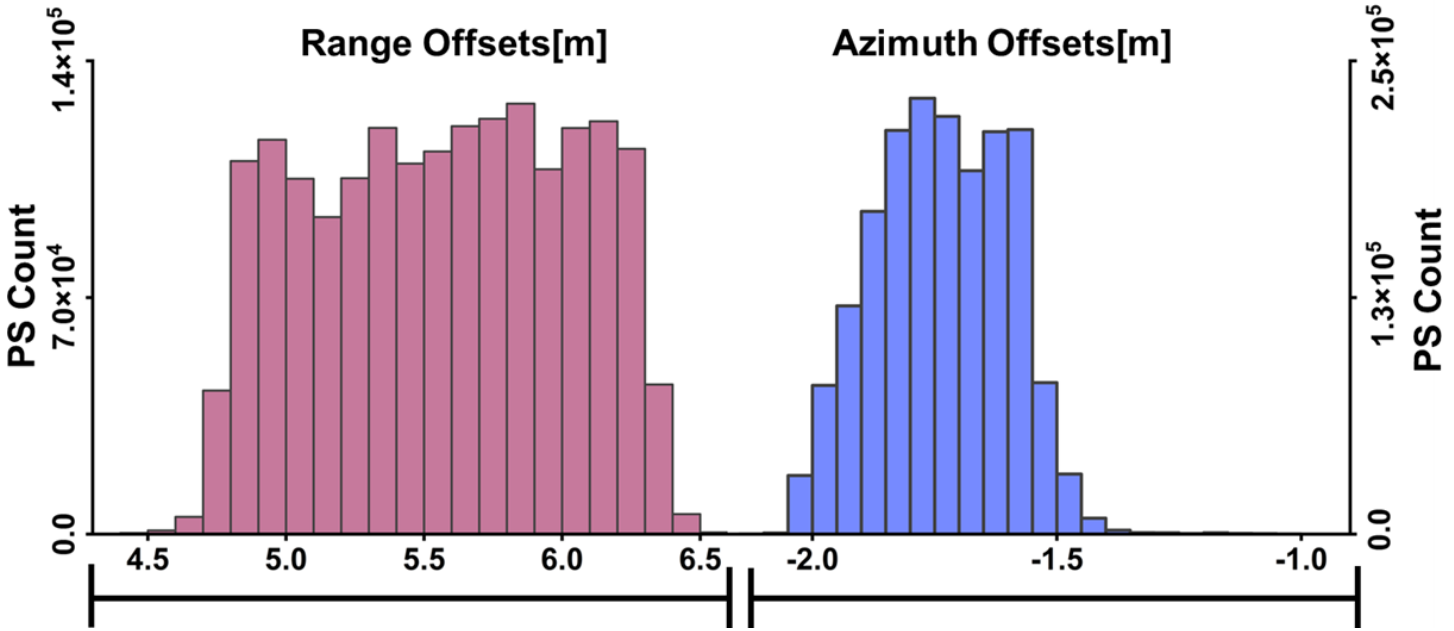
Mean： 1.7

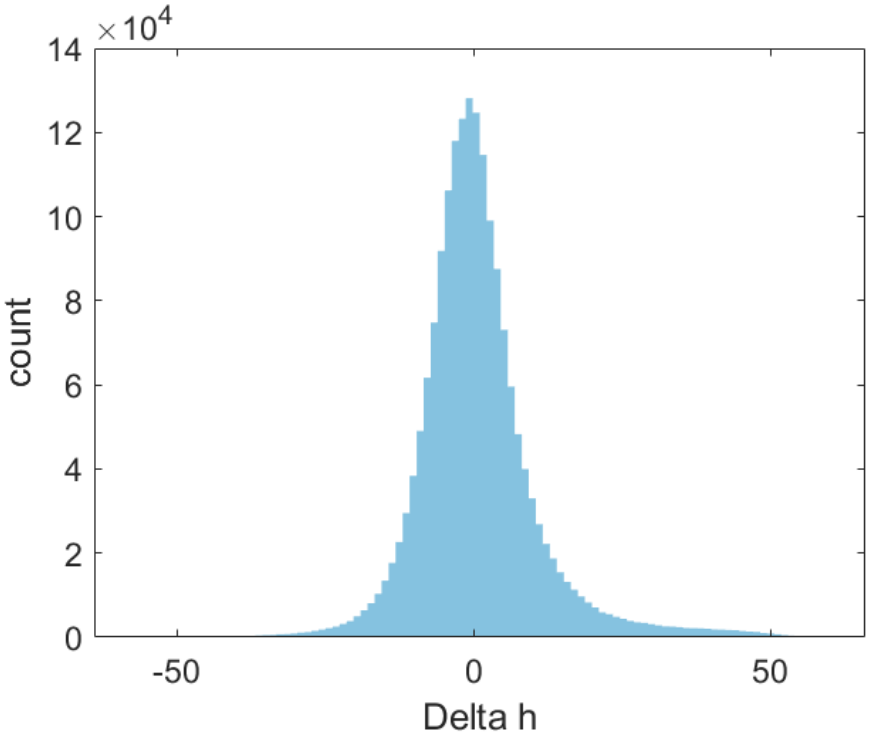
Std dev： 0.1

$\Delta h[m]$:

Mean： 0.6

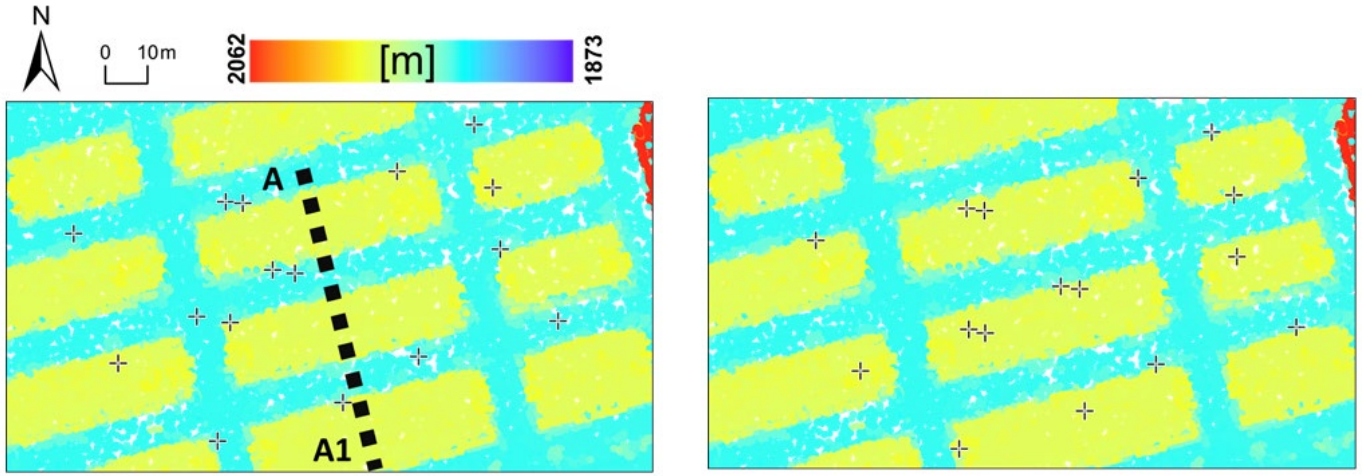
Std dev： 10.1

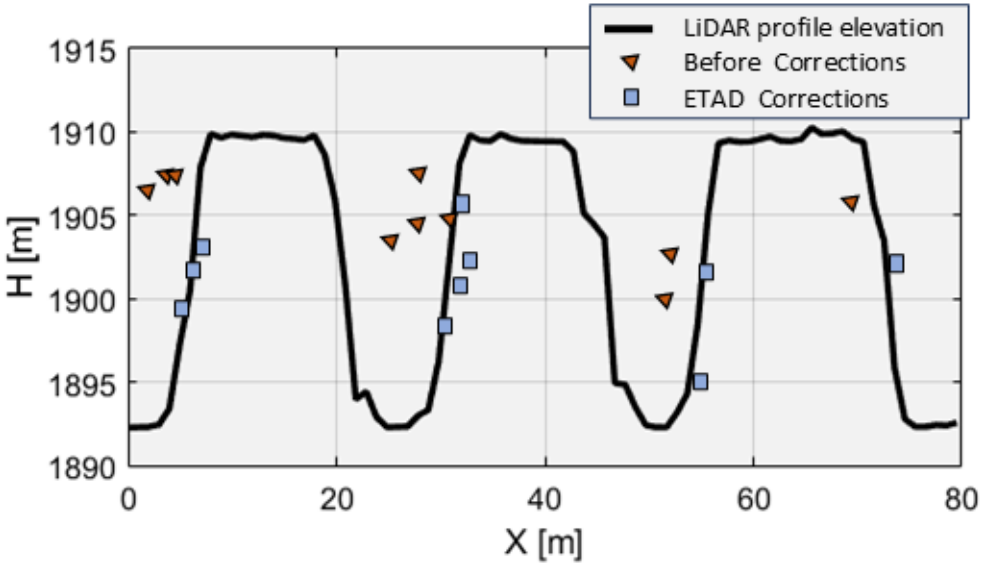




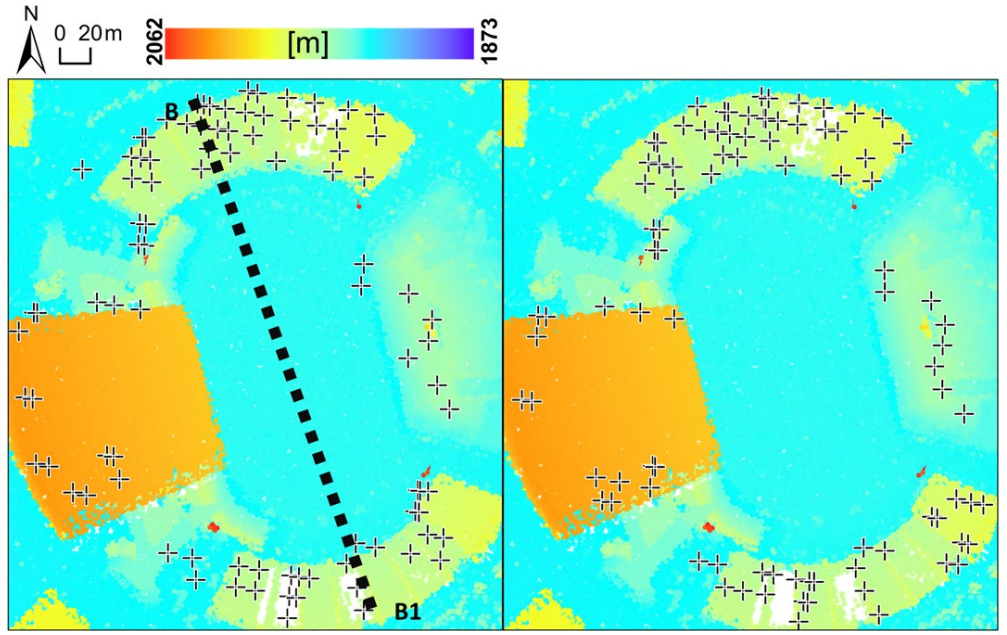
Results-geolocation

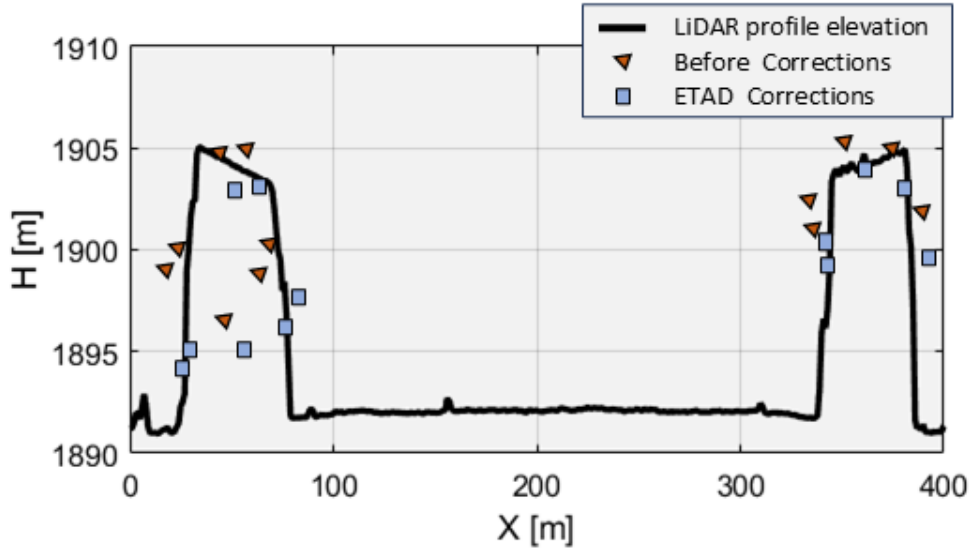
AREA1:





AREA2:





Conclusions part 1

Through the evaluation of results and indicators

After being corrected by ETAD

- Interferogram
- Velocity
- time series
- geolocation

…yhey have all improved to some extent.

In summary, introducing ETAD products into the PSI data processing flow can effectively reduce errors in S1 data processing.

Overview of Chinese YSs research

2. Railway Deformation Zone Mapping via InSAR Phase Gradient Stacking: Chinese Section of China-Laos Railway

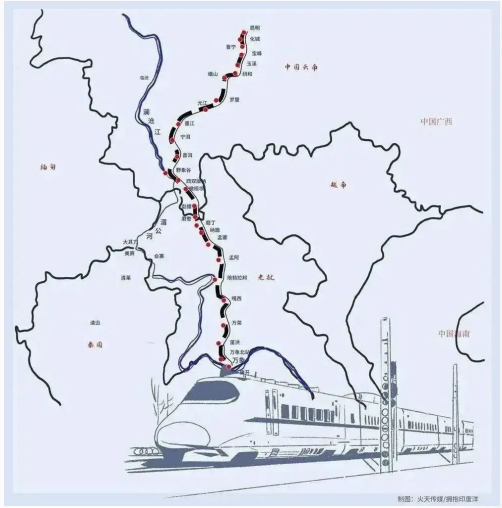
- In this study, we apply phase stacking techniques to identify potential hazard zones along the China-Laos Railway.
- We first analyze the influence of stacking step size and interferogram selection on the results and subsequently detect potential geohazard-prone areas along the railway corridor.

Railway Deformation Zone Mapping via InSAR Phase Gradient Stacking: Chinese Section of China-Laos Railway

➢ The **safe operation** of **high-speed railways** throughout their life cycle is critical, given their essential role in modern transportation systems.



Framework of China's High-Speed Railway Network



Alignment Map of the China-Laos Railway

Characteristics of High-Speed Railway Infrastructure

①Long-distance and large spatial span;

②Traversing mountainous areas, fault zones, and soft soil areas

Complex Geological and Geotechnical Constraints

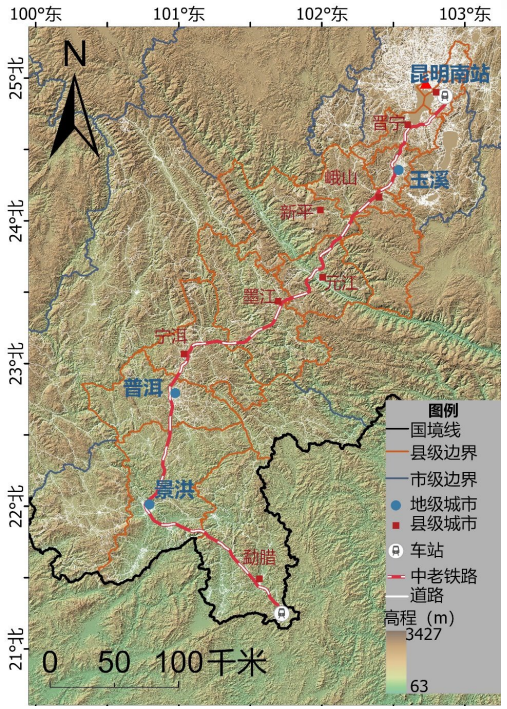
Poses Safety Challenges



Potential geological hazards pose ongoing challenges to the safe operation of high-speed railways and EMU trains. Thus, conducting surface deformation monitoring studies along railway corridors is crucial to identify potentially unstable areas and mitigate disaster impacts.

Railway Deformation Zone Mapping via InSAR Phase Gradient Stacking: Chinese Section of China-Laos Railway

The China-Laos Railway (Kunming-Vientiane Railway) connects Kunming, China to Vientiane, Laos, with its Chinese section (Kunming to Mohan) spanning 586 km.

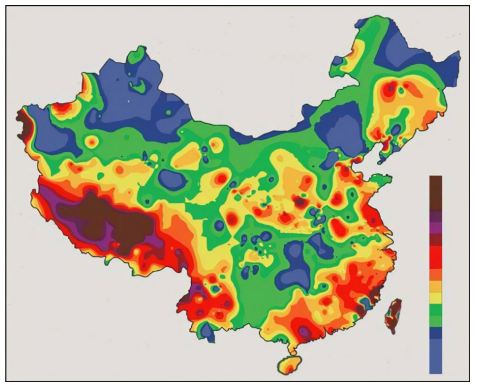


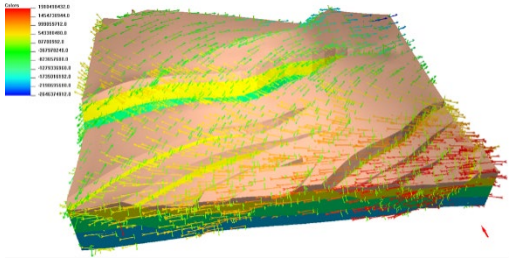
Traversing the "Three Critical Mountain Ranges": Mopan, Ailao, and Wuliang Mountains.

Crossing the "Four Major River Systems": Yuanjiang, Mojiang, Babianjiang, and Lancang Rivers.

Interlaced by towering mountains, incised valleys, and plateau "intermontane basins" (bazi), the region exhibits remarkable geomorphological diversity of tectonic origin.

High Geothermal Anomalies; Elevated In-Situ Stresses; High Seismic Intensity





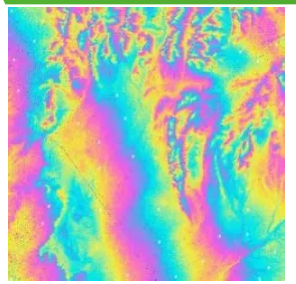
The complex geological setting has engendered a railway engineering marvel, while imposing heightened requirements for ongoing structural monitoring.

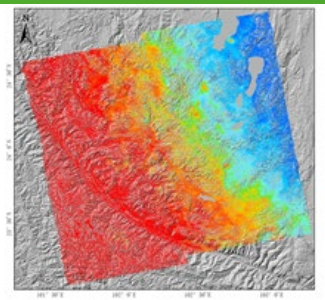
Employing InSAR phase gradient stacking to map surface deformation fields along the corridor, we integrate geomorphological data and optical imagery to identify potentially unstable zones—with particular focus on slope instabilities and ground subsidence—and analyze their spatiotemporal developmental patterns.

Methodology

- Compared to TS-InSAR techniques, IPGS offers superior performance for deformation monitoring and early-stage geohazard identification along railway corridors.

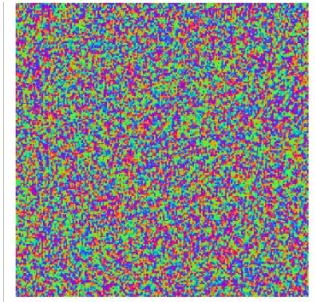
Technical Advantages



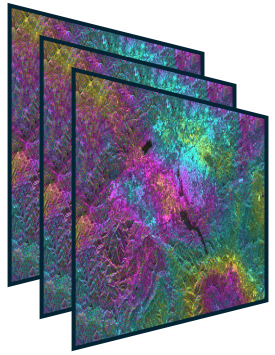


- High Efficiency
- Effective Atmospheric Noise Suppression

Constructing an Effective Railway Deformation Gradient Field



Phase component



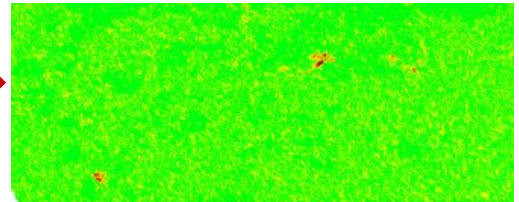
- IPGS operates by directly retrieving deformation from phase signals.
- Generating Interferometric Pairs via SBAS and Processing with IPGS to Derive Deformation Information

$$\Delta\varphi_i^{se}(m,n) = \mathrm{Wrap}[\varphi_i(m+s,n+s)] - \varphi_i(m,n)]$$

$$\Delta\varphi^{se}(m,n) = \sum_i^M \Delta\varphi_i^{se}(m,n)$$

$$\varphi = \sqrt{\frac{\Delta\varphi^{e\,2} + \Delta\varphi^{s\,2} + \Delta\varphi^{se\,2} + \Delta\varphi^{ne\,2}}{4}}$$

$$\emptyset_i = \frac{\varphi_i - \varphi_{min}}{\varphi_{max} - \varphi_{min}}$$



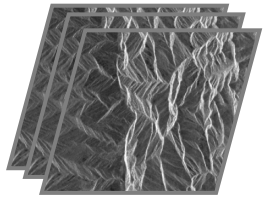
Results of IPGS

Methodology

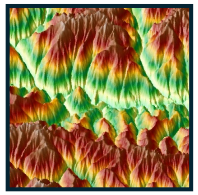
Implementation Workflow

Software Platform

SBAS-InSAR



Raw SAR data



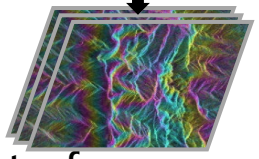
DEM data

Co-registration

Selection of Image Pairs

Geocoding

Interferogram Generation



Interferograms

GAMMA

Phase Gradient Stacking

Set Parameters

Step

Interferogram

Filtering Window

Mask Parameters

Direction

Gradient Calculation

N

E

SE

NE

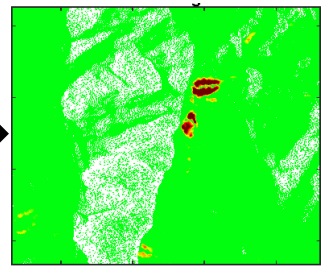
Gradient Stacking

Stacking

Filtering

Fusion

Stretching



MATLAB

Result Visualization

Data Processing

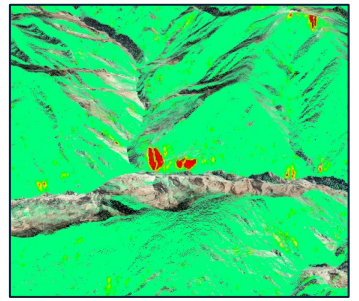
Data Conversion

Geocoding

Multi-track Mosaicking

Mapping

Result



ArcGIS/Google Earth

Methodology

✅ Introducing Ground Distance to Calibrate Phase Gradient Calculations for Mitigating Geometric Distortions

$$\Delta\varphi_i^{se}(m,n)' = \frac{\mathrm{Wrap}\{\varphi_i(m+s,n+s) - \varphi_i(m-s,n-s)\}}{\sqrt{\left(X_{(m+s,n+s)} - X_{(m-s,n-s)}\right)^2 + \left(Y_{(m+s,n+s)} - Y_{(m-s,n-s)}\right)^2}}$$

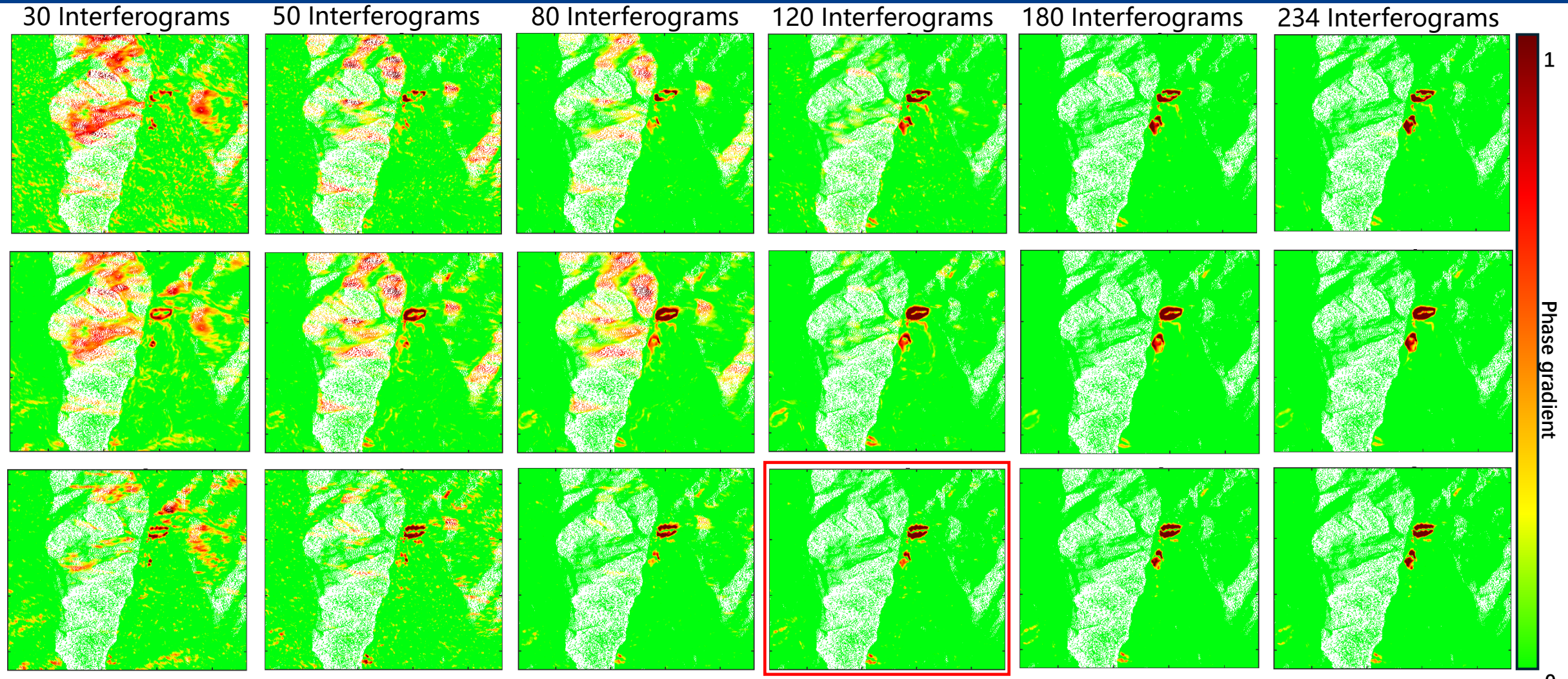
Where $\Delta\varphi_i^{se}(m,n)'$ is the phase gradient of a pixel in the southeast direction, $\varphi(,)$ represents the wrapped phase of the corresponding pixel, $Wrap(\cdot)$ denotes the phase wrapping operation, s is the step size, and X, Y are the projected local coordinates.

✅ Using coherence to weight the phase gradient results for suppressing random noise.

$$\Delta\varphi_i^{se}(m,n) = \begin{cases} \Delta\varphi_i^{se}(m,n)' \times \dfrac{c_{(m+s,n+s)} + c_{(m-s,n-s)}}{2}, & c_{(m+s,n+s)} \geq 0.2 \ and \ c_{(m+s,n+s)} \geq 0.2 \\ 0, & c_{(m+s,n+s)} < 0.2 \ \ or \ c_{(m+s,n+s)} < 0.2 \end{cases}$$

Where $\Delta\varphi_i^{se}(m,n)$ is the coherence-weighted phase gradient of a pixel in the southeast direction, and $c(m,n)$ is the coherence of the corresponding pixel.

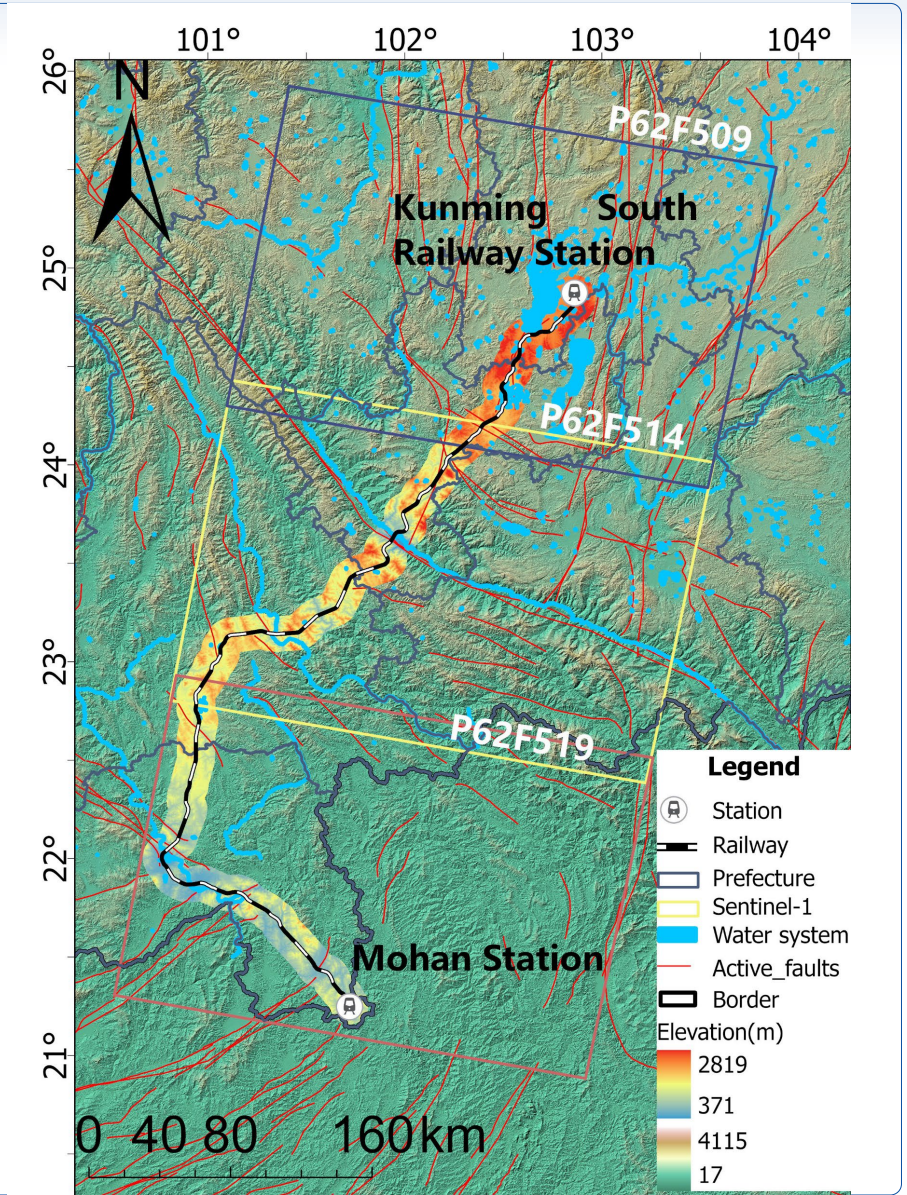
Methodology-testing on num of ifg & weighting strategy



- Coherence weighting can effectively suppress the impact of random noise.
- Applying ground-range correction to the PGS results can effectively address the issue of false deformation introduced by traditional methods in foreshortening regions.

Experiments

Study Area



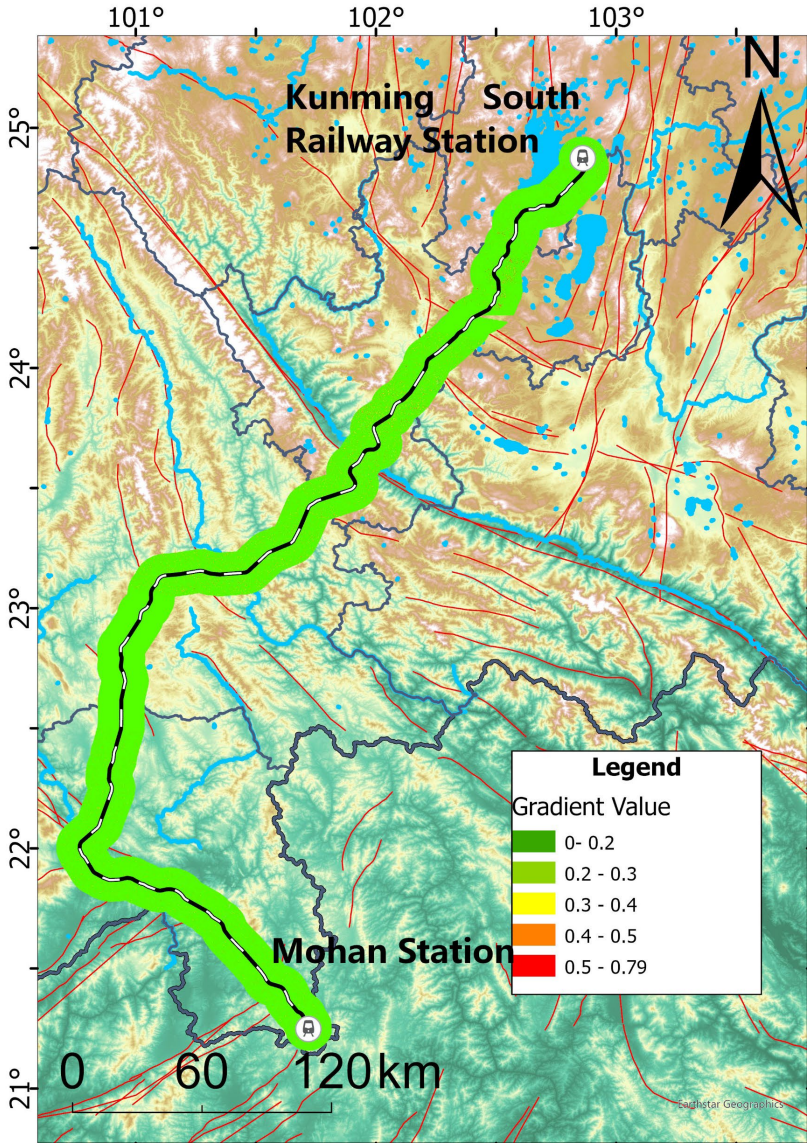
- Utilizing Sentinel-1 descending orbit data covering the study area (2022-2024)

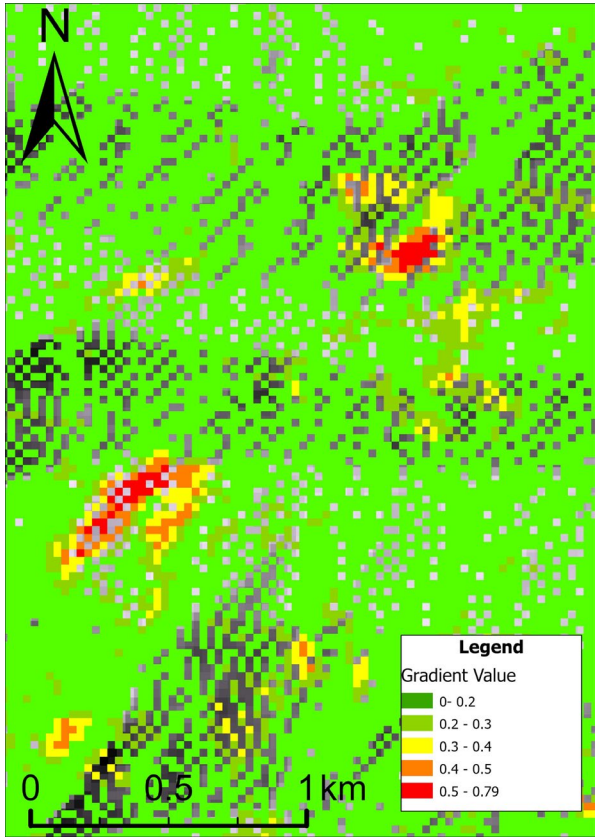
Data Parameters

Orbit	Descending		
Time	2022.1.12—2024.12.27		
Path	62	62	62
Frame	509	514	519
Quantity	87	87	87

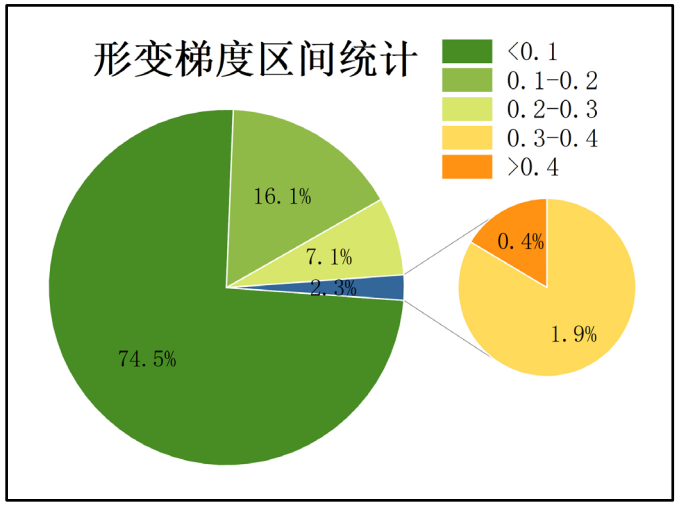
Experiments- Preliminary results

Full-Section Deformation Gradient Results





➢ Local Deformation



- 75% of the area shows minimal deformation (gradient <0.1),
- 16% is under slight deformation,
- 7% under moderate (0.3–0.4),
- 2% under relatively strong deformation (>0.4).

European Young Scientists contributions in Dragon 6

Name	Institution	Poster title	Contribution including period of research
Lina Hagenah1, Wietske Brouwer1, Yuqing Wang1, Mengshi Yang2, Wouter Niessen1, Antonio Napolitano3, Ramon Hanssen1	1Delft University of Technology, The Netherlands, Netherlands, The; 2Yunnan University (YNU), China; 3University Roma Tre, Italy	Taking INSAR Point Scatterers to the Max: Optimizing the Interpretation of a Single Scatterer in Terms of Information	

Chinese Young Scientists contributions in Dragon 6

Name	Institution	Poster title	Contribution including period of research
Yangwei Yu1, Mengshi Yang1, Ramon F Hanssen2, Yuqing Wang2, Lina Hagenah2, Kang Yin1, Weibin Huang1, Hao Wu1, Siran Chen	1Yunnan University, China, China, People's Republic of; 2Delft University of Technology The Netherlands	Railway Deformation Zone Mapping via InSAR Phase Gradient Stacking: Chinese Section of China-Laos Railway	

Publications list

[1] Huang Yiming, Yang Mengshi*, Huang Cheng, Liu Zhaohai, Zhao Zhifang. Identification and Sensitivity Modeling of InSAR Geometric Distortions along the China-Laos Railway Corridor [J]. Geospatial Information, 2025. In Chinese [黄一鸣; 杨梦诗*; 黄成; 刘朝海; 赵志芳. 中老铁路沿线InSAR监测几何畸变判识与灵敏度建模[J]. 地理空间信息, 2025.]

[2] Mengshi Yang, Saiwei Li, and Hang Yu, A Transfer Learning Approach for Deformation Pattern Recognition in InSAR Time Series, IEEE Transactions on Geoscience and Remote Sensing, vol. 63, pp. 1-16, 2025.

[3] Yang, M.; Li, M.*; Huang, C.; Zhang, R.; Liu, R. Exploring the InSAR deformation series using unsupervised learning in a built environment[J]. Remote Sensing, 2024, 16: 1375.

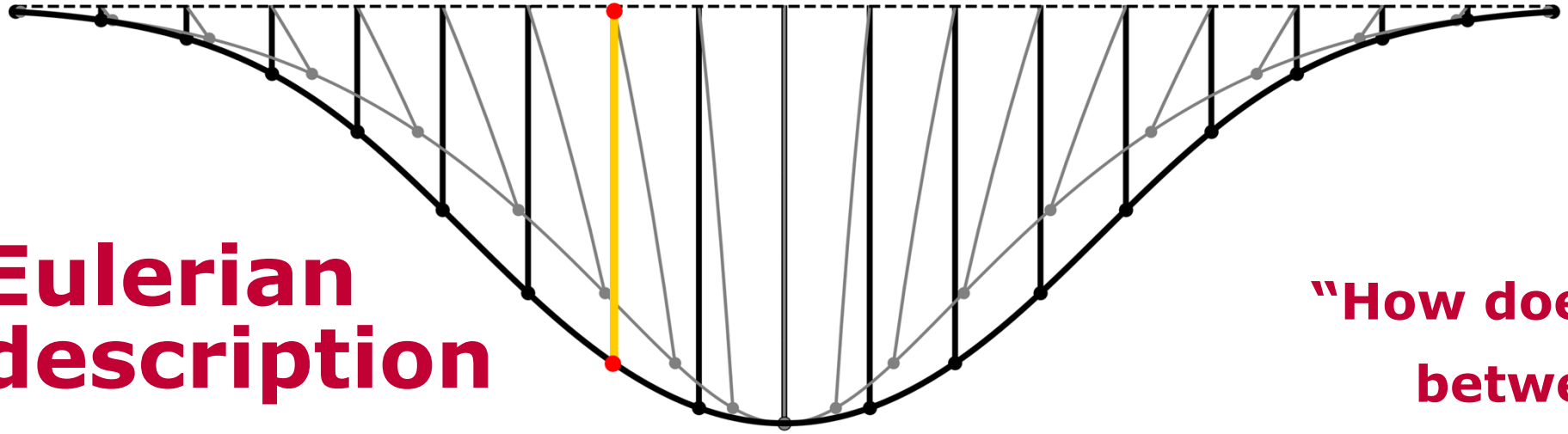
[4] Li, M.; Gao, X.; Yang, M.; Tang, L.; Tang, B.-H. Evaluating the stability of architectural heritage from the perspective of InSAR: A practical study on Jianchuan Ancient Town[J]. Heritage Science, 2024, 12(3): 2050-7445.

Overview of European YSs research

Overview of European YSs research (when applicable)

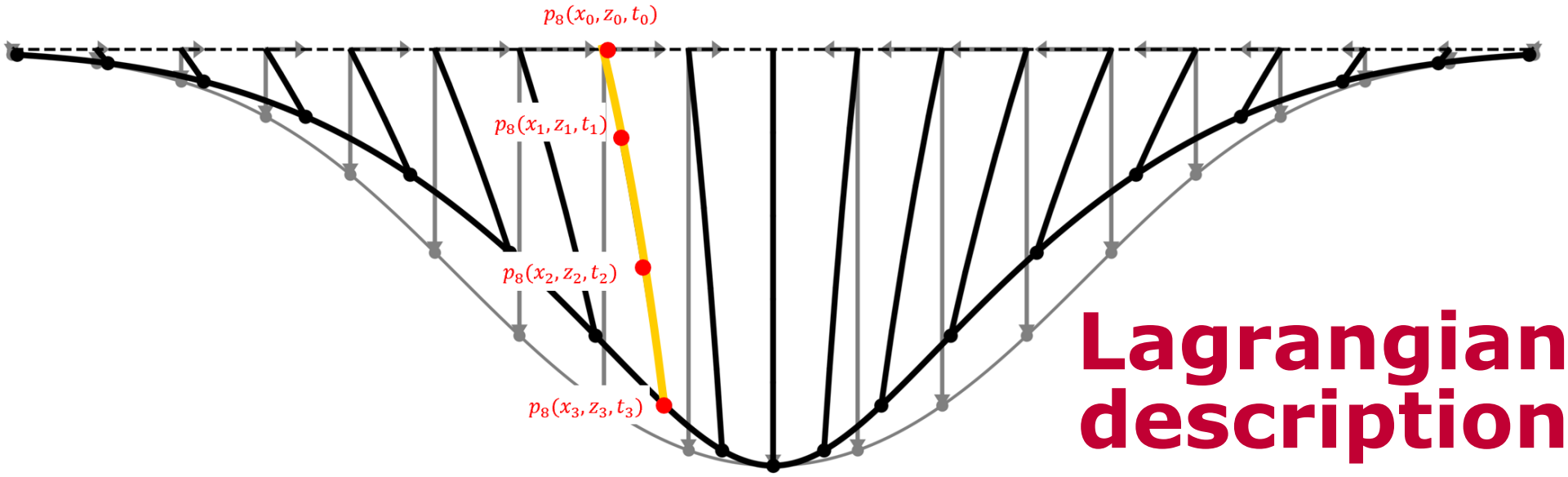
The strapdown method : 2DL/3DG

"How does the elevation change for a particular horizontal coordinate?"



Eulerian description

"How does a particle move between t_0 and t_1?"



t_0

t_1 (Eulerian)

t_1 (Lagrangian)

Lagrangian description

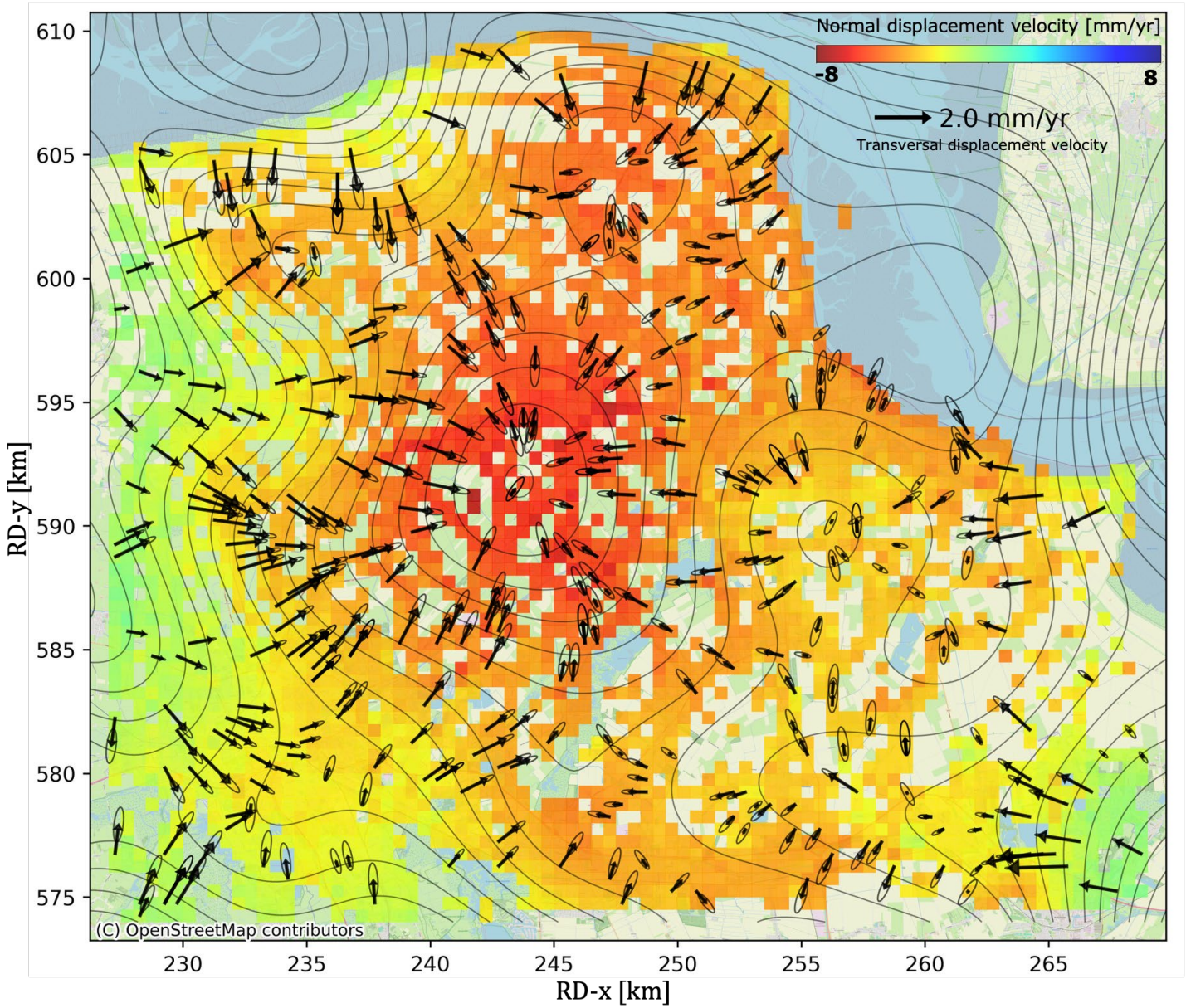
Journal of Geodesy (2024) 98:110
https://doi.org/10.1007/s00190-024-01918-2

ORIGINAL ARTICLE

Estimating three-dimensional displacements with InSAR: the strapdown approach

Wietske S. Brouwer[1] · Ramon F Hanssen[1]

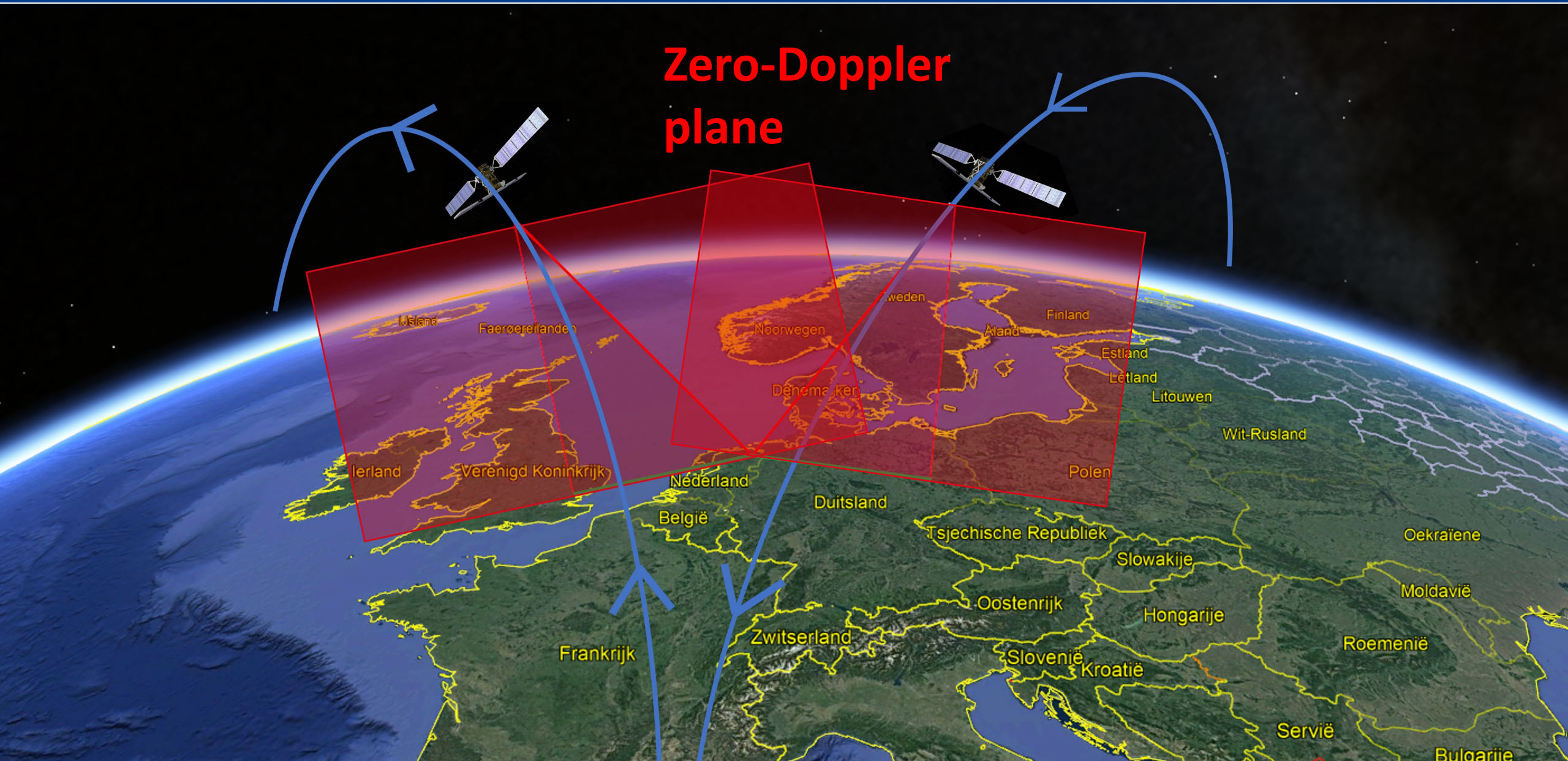
The strapdown method : 2DL/3DG





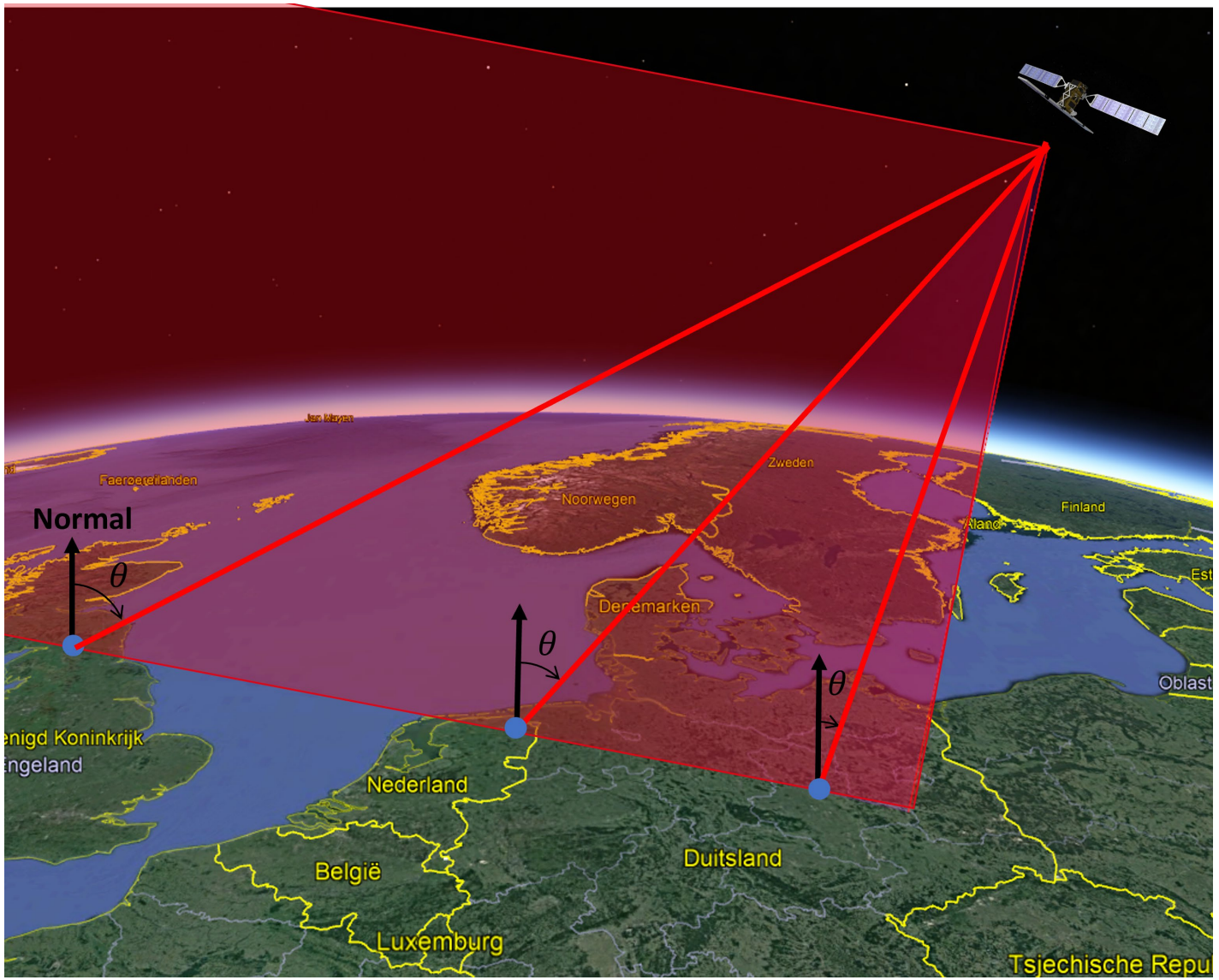
2-sigma error elllipses →
95% confidence regions

The geometry



The viewing geometry: Incidence angle θ

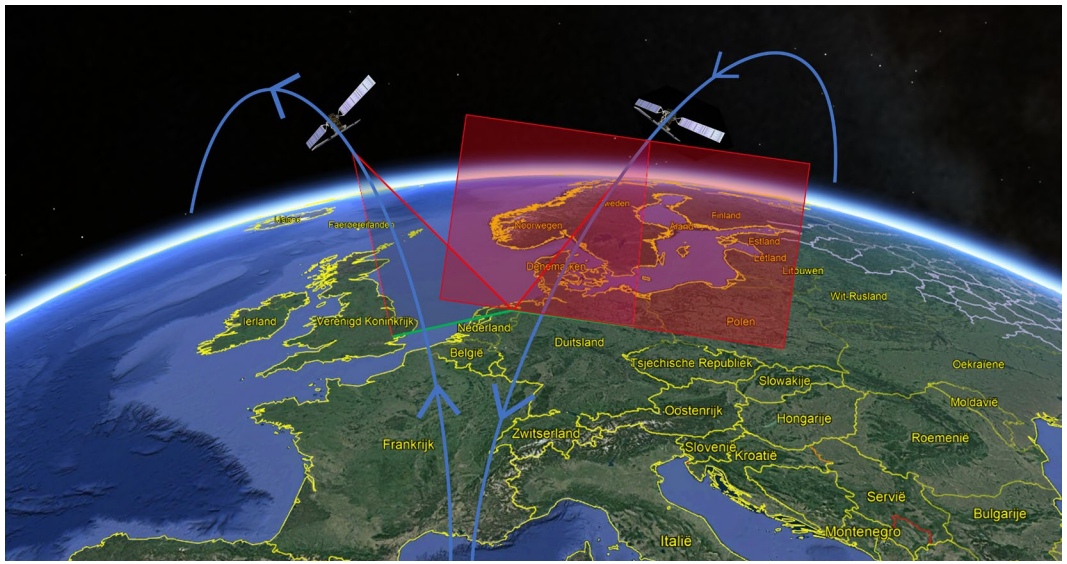
Far range



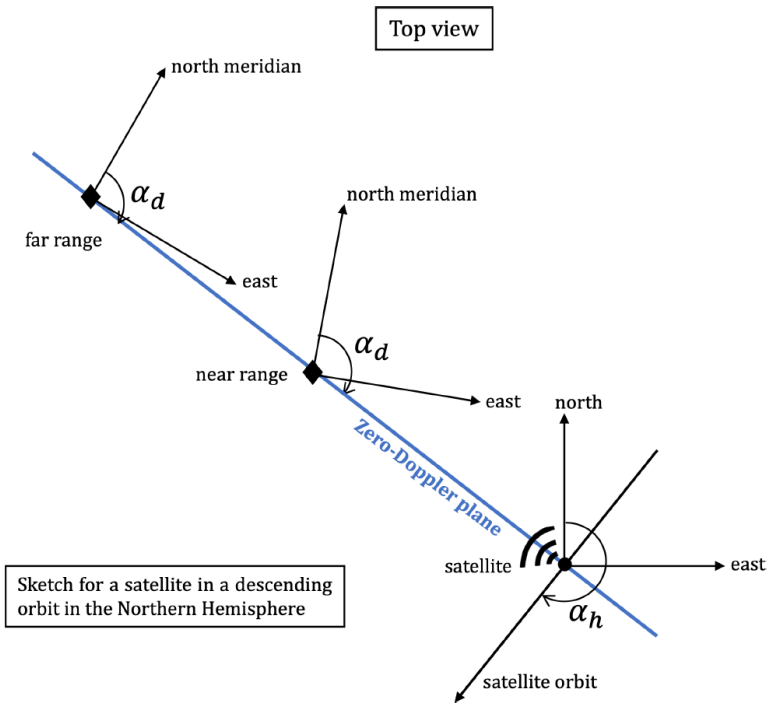
Near range

The viewing geometry: heading angle α_h

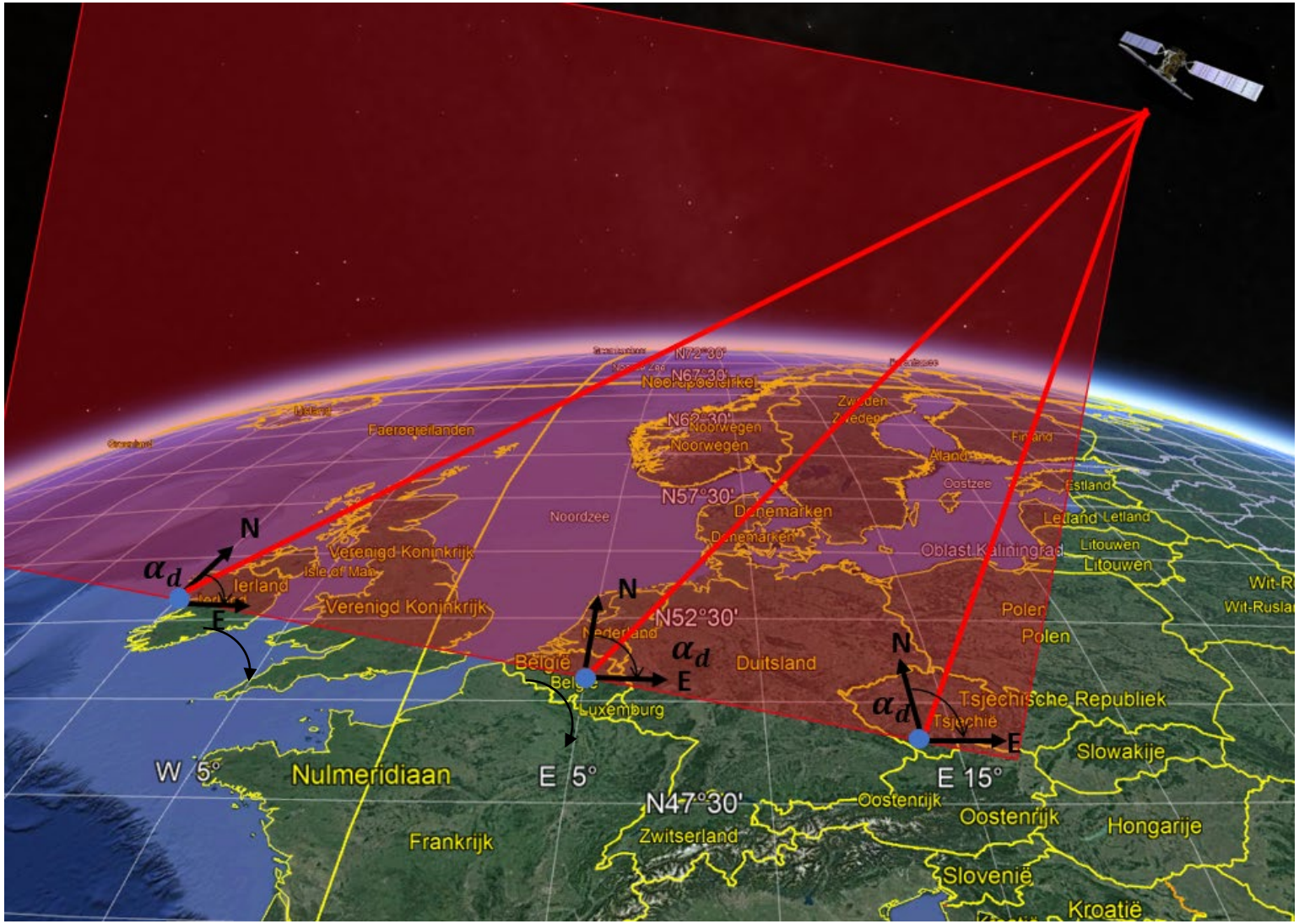




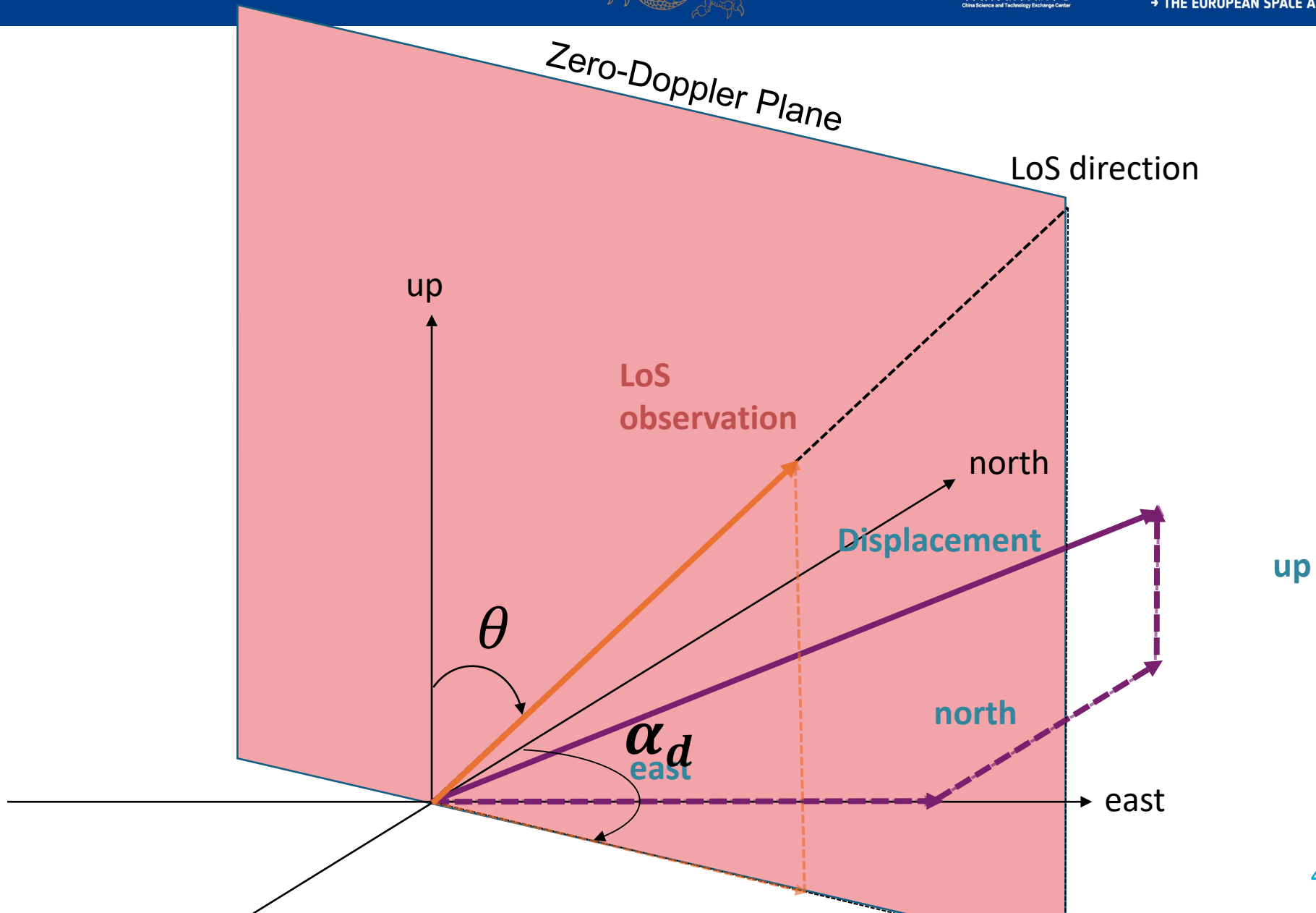
The viewing geometry: azimuth of the zero-Doppler plane



Sketch for a satellite in a descending orbit in the Northern Hemisphere



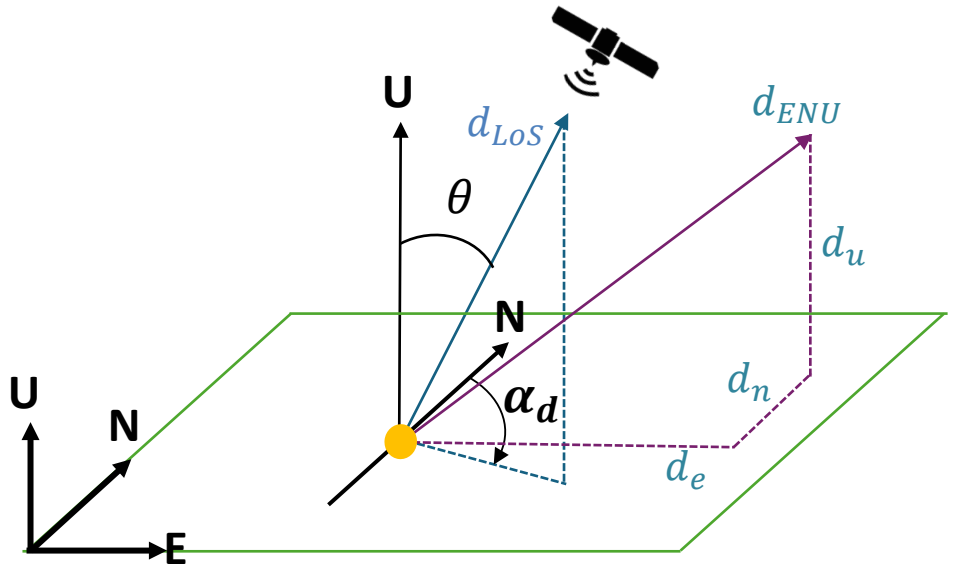
Line-of-Sight (LoS)



The geometry

$$d_{\mathrm{LoS}} = \begin{bmatrix} \sin(\theta)\ \sin(\alpha_d) & \sin(\theta)\ \cos(\alpha_d) & \cos(\theta) \end{bmatrix} \begin{bmatrix} d_e \\ d_n \\ d_u \end{bmatrix}$$

InSAR satellite observation



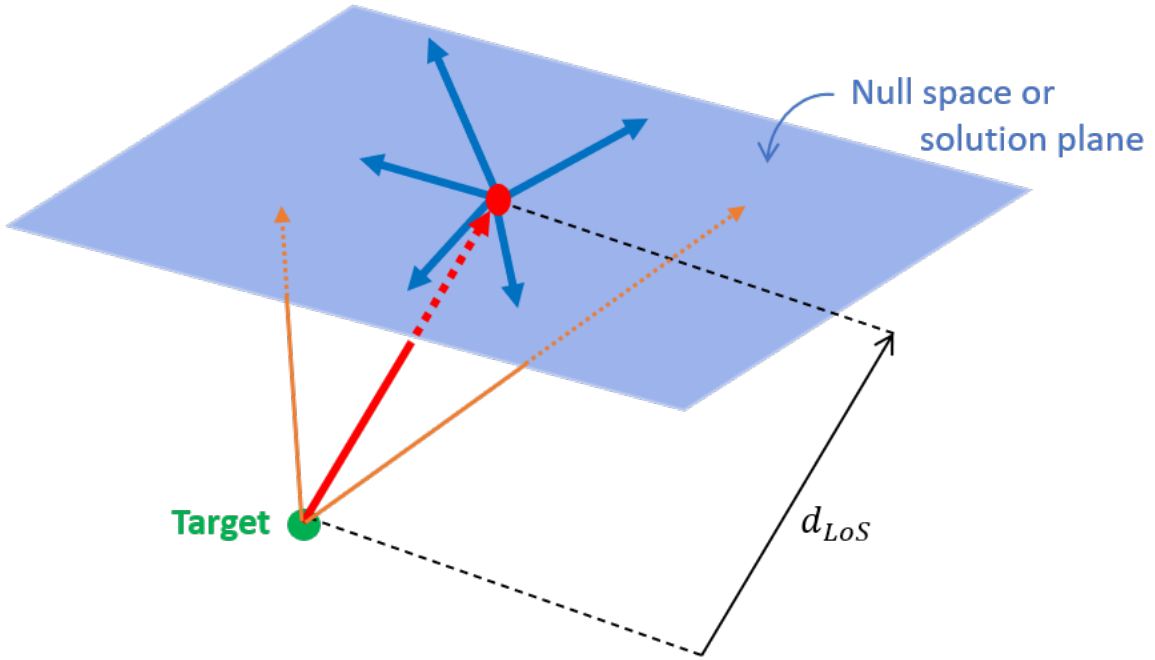
Real world displacements: Parameters of interest

TU Delft

The geometry

$$E\{\underbrace{\left[\underline{d}_{\mathrm{LoS}}^{(1)}\right]}_{y}\} = \underbrace{\left[\sin(\theta_1)\ \sin(\alpha_{d,1}) \quad \sin(\theta_1)\ \cos(\alpha_{d,1}) \quad \cos(\theta_1)\right]}_{A} \underbrace{\begin{bmatrix} d_e \\ d_n \\ d_u \end{bmatrix}}_{x}$$

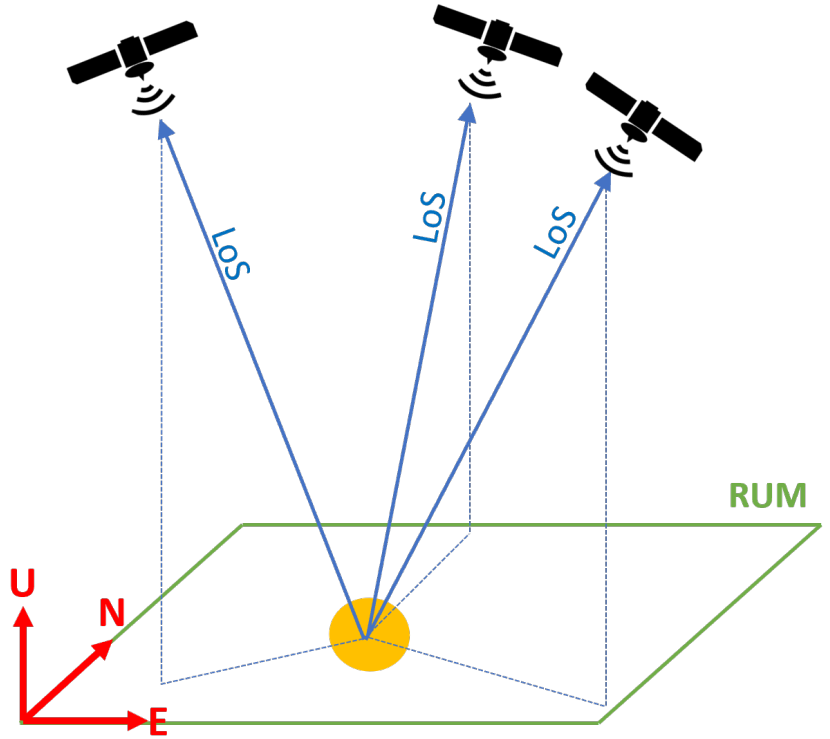
1 satellite observation



Real world displacements: Parameters of interest

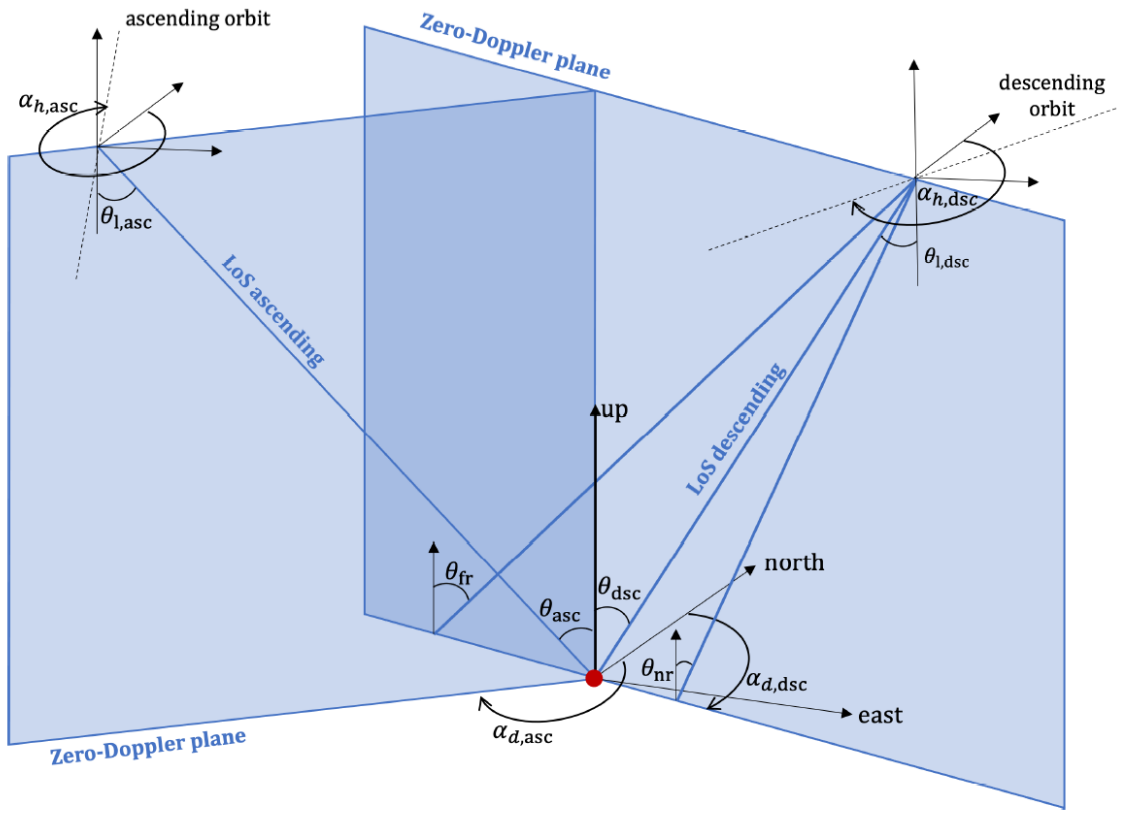
The geometry

$$E\{\underbrace{\begin{bmatrix} d_{\mathrm{LoS}}^{(1)} \\ d_{\mathrm{LoS}}^{(2)} \\ \vdots \\ d_{\mathrm{LoS}}^{(m)} \end{bmatrix}}_{y}\} = \underbrace{\begin{bmatrix} \sin(\theta_1) & \sin(\alpha_{d,1}) & \sin(\theta_1)\cos(\alpha_{d,1}) & \cos(\theta_1) \\ \sin(\theta_2) & \sin(\alpha_{d,2}) & \sin(\theta_2)\cos(\alpha_{d,2}) & \cos(\theta_2) \\ & \vdots & \vdots & \vdots \\ \sin(\theta_m) & \sin(\alpha_{d,m}) & \sin(\theta_m)\cos(\alpha_{d,m}) & \cos(\theta_m) \end{bmatrix}}_{A} \underbrace{\begin{bmatrix} d_e \\ d_n \\ d_u \end{bmatrix}}_{x}$$



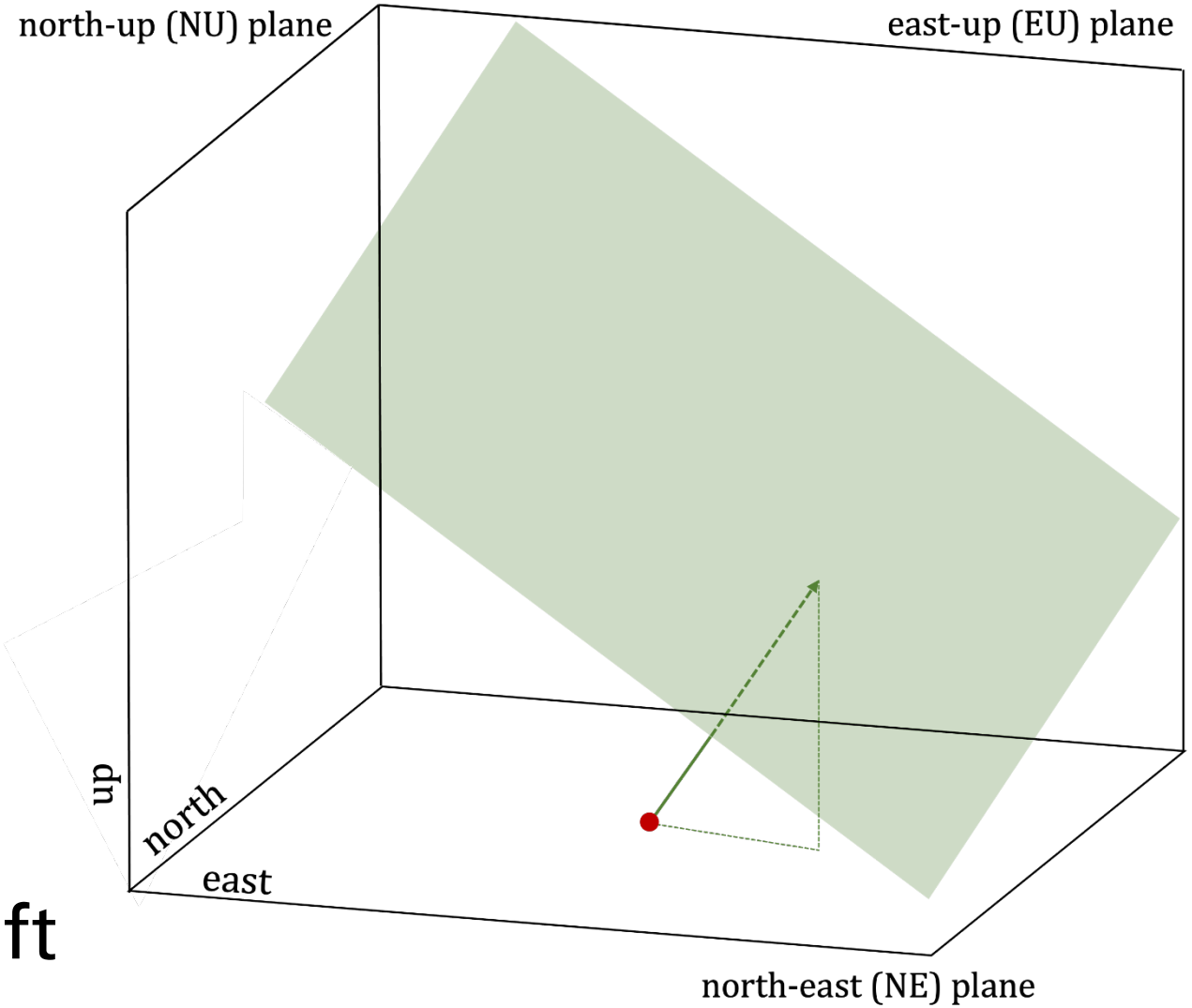
An underdetermined problem

$$E\{\underbrace{\begin{bmatrix} d^{\text{asc}}_{\text{LoS}} \\ d^{\text{dsc}}_{\text{LoS}} \end{bmatrix}}_{y}\} = \underbrace{\begin{bmatrix} \sin(\theta_1)\ \sin(\alpha_{d,1}) & \sin(\theta_1)\ \cos(\alpha_{d,1}) & \cos(\theta_1) \\ \sin(\theta_2)\ \sin(\alpha_{d,2}) & \sin(\theta_2)\ \cos(\alpha_{d,2}) & \cos(\theta_2) \end{bmatrix}}_{A} \underbrace{\begin{bmatrix} d_e \\ d_n \\ d_u \end{bmatrix}}_{x}$$



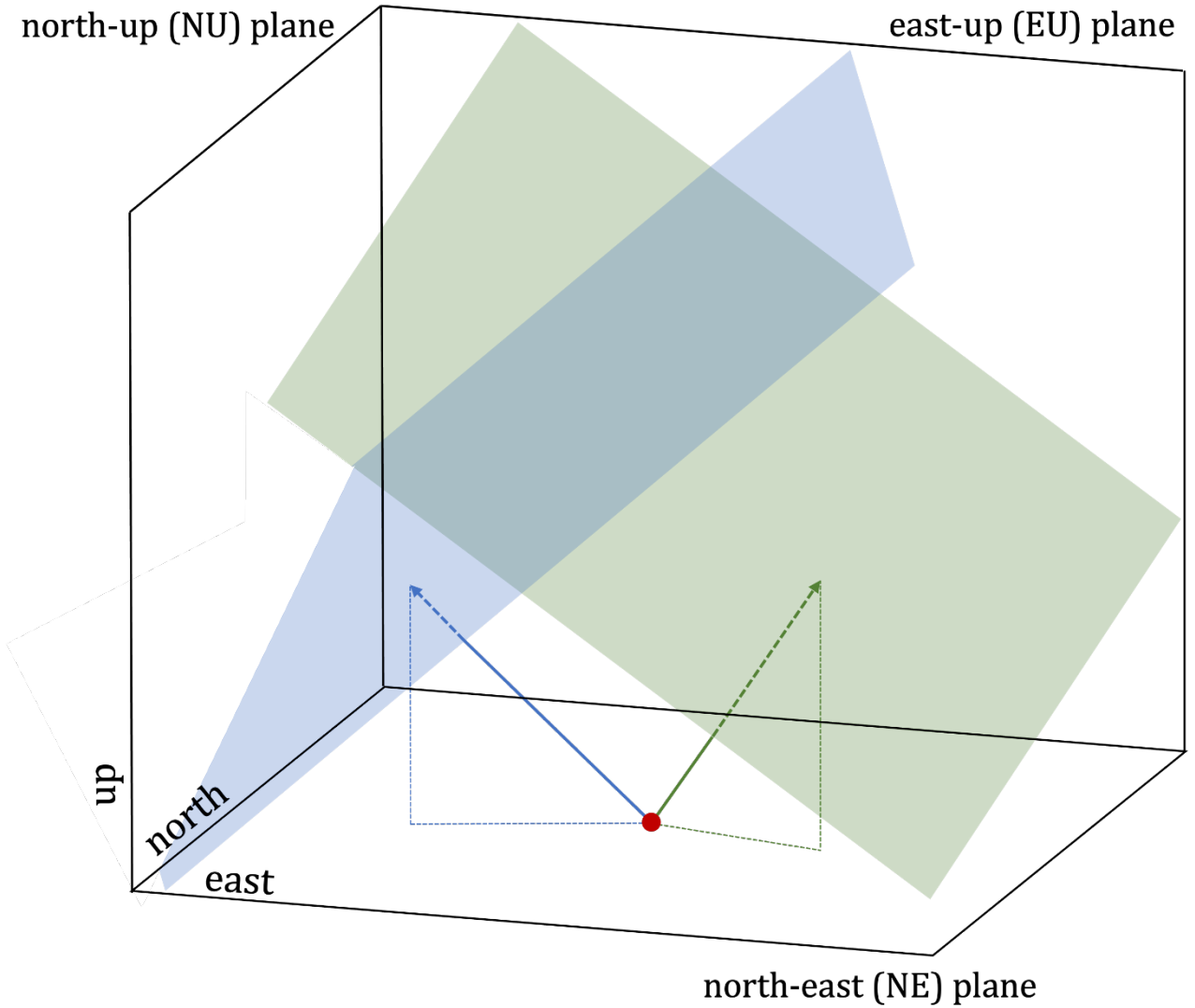
1 LoS observation

$$d_{\mathrm{LoS}} = \begin{bmatrix} \sin(\theta)\ \sin(\alpha_d) & \sin(\theta)\ \cos(\alpha_d) & \cos(\theta) \end{bmatrix} \begin{bmatrix} d_e \\ d_n \\ d_u \end{bmatrix}$$



2 LoS observations

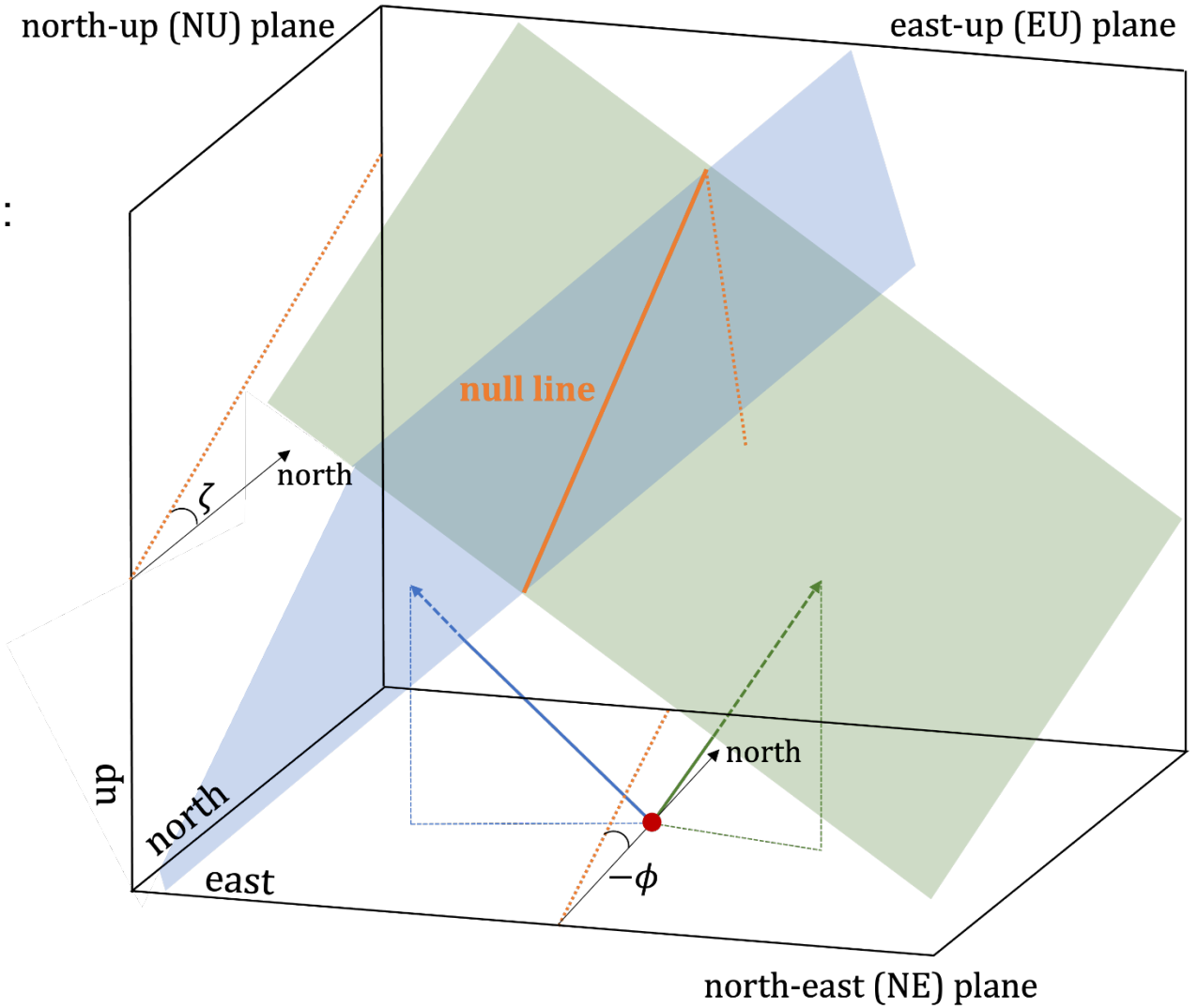
$$E\{\underbrace{\begin{bmatrix} d_{\mathrm{LoS}}^{\mathrm{asc}} \\ d_{\mathrm{LoS}}^{\mathrm{dsc}} \end{bmatrix}}_{y}\} = \underbrace{\begin{bmatrix} \sin(\theta_1) & \sin(\alpha_{d,1}) & \sin(\theta_1)\cos(\alpha_{d,1}) & \cos(\theta_1) \\ \sin(\theta_2) & \sin(\alpha_{d,2}) & \sin(\theta_2)\cos(\alpha_{d,2}) & \cos(\theta_2) \end{bmatrix}}_{A} \underbrace{\begin{bmatrix} d_e \\ d_n \\ d_u \end{bmatrix}}_{x}$$



The null line

Described by two angles:

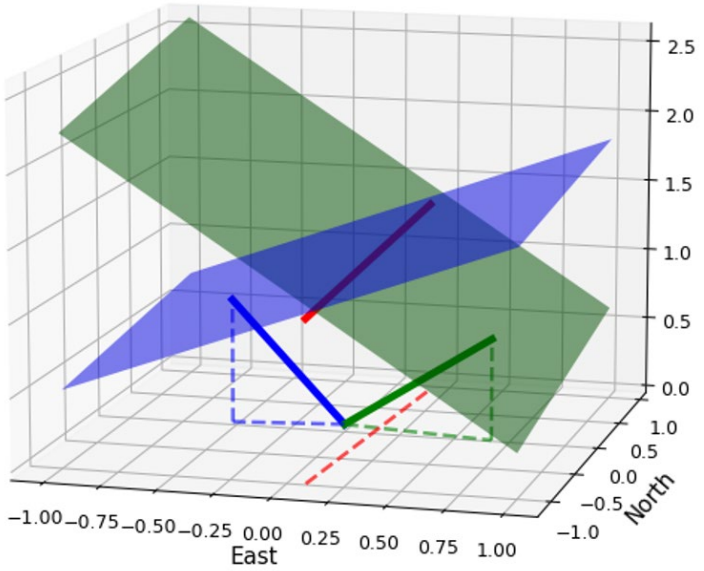
- Azimuth angle ϕ
- Elevation angle ζ

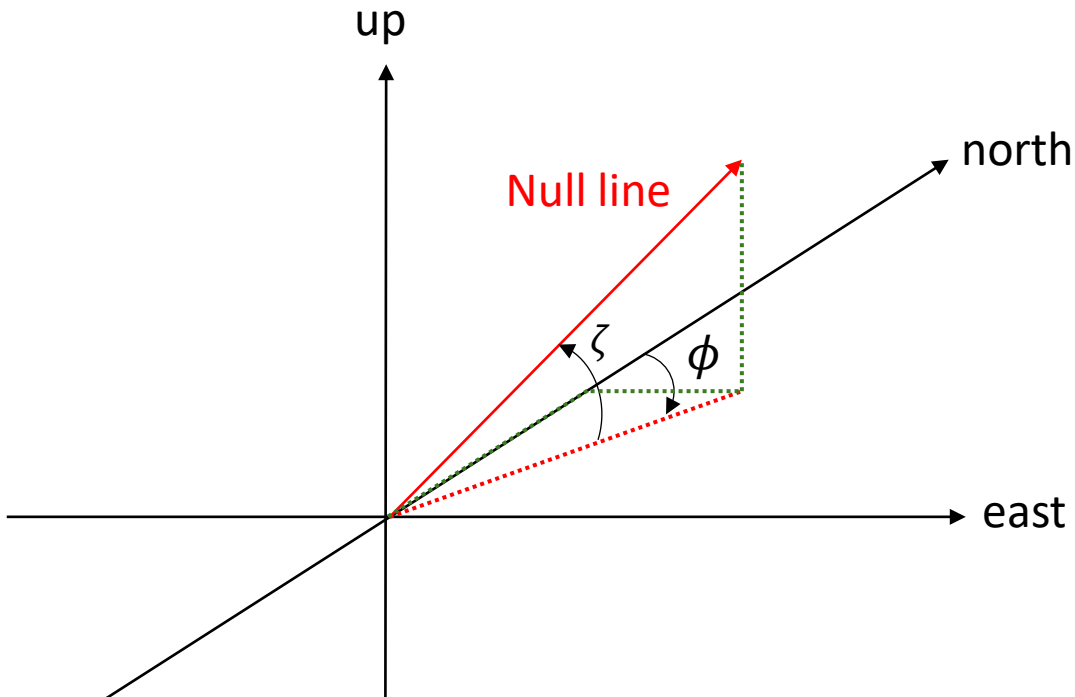


The underdetermined problem

$$E\{\underbrace{\begin{bmatrix} d^{asc}_{LoS} \\ d^{dsc}_{LoS} \end{bmatrix}}_{y}\} = \underbrace{\begin{bmatrix} \sin(\theta_1)\ \sin(\alpha_{d,1}) & \sin(\theta_1)\ \cos(\alpha_{d,1}) & \cos(\theta_1) \\ \sin(\theta_2)\ \sin(\alpha_{d,2}) & \sin(\theta_2)\ \cos(\alpha_{d,2}) & \cos(\theta_2) \end{bmatrix}}_{A} \underbrace{\begin{bmatrix} d_e \\ d_n \\ d_u \end{bmatrix}}_{x}$$

Underdetermined problem: infinite number of solutions, along the "null line"



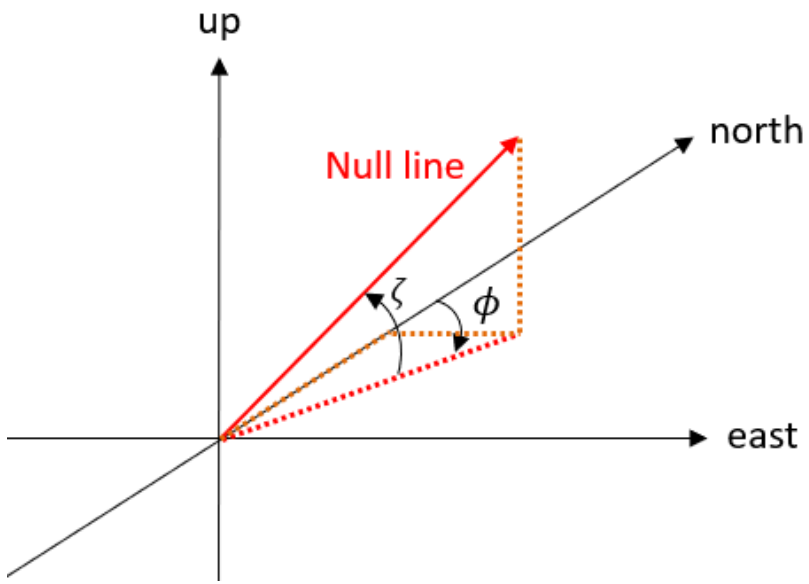


Conventional (biased) 2D decomposition

$$E\{\underbrace{\begin{bmatrix} d^{(1)}_{\mathrm{LoS}} \\ d^{(2)}_{\mathrm{LoS}} \end{bmatrix}}_{y}\} = \underbrace{\begin{bmatrix} \sin\theta_1 & \sin\alpha_{d,1} & \cos\theta_1 \\ \sin\theta_2 & \sin\alpha_{d,2} & \cos\theta_2 \end{bmatrix}}_{A} \underbrace{\begin{bmatrix} d_e \\ d_u \end{bmatrix}}_{x}$$

Decomposition error!

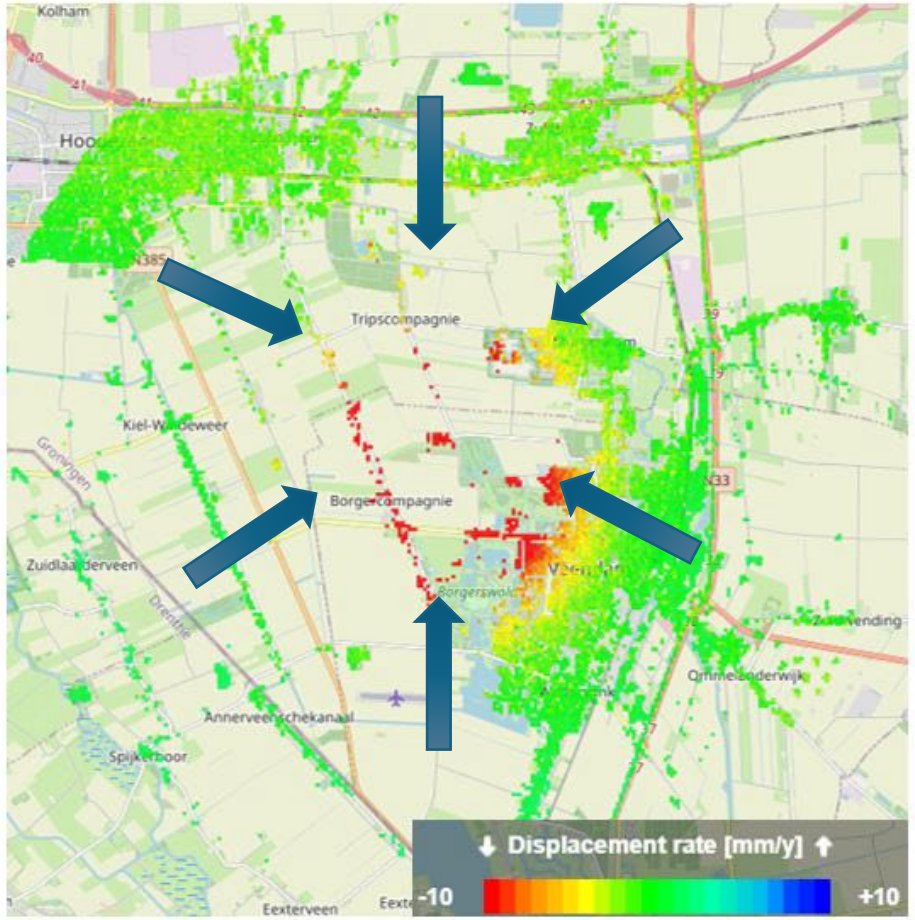
Solution line for the underdetermined problem



Orientation of the line → Up and/or East biased

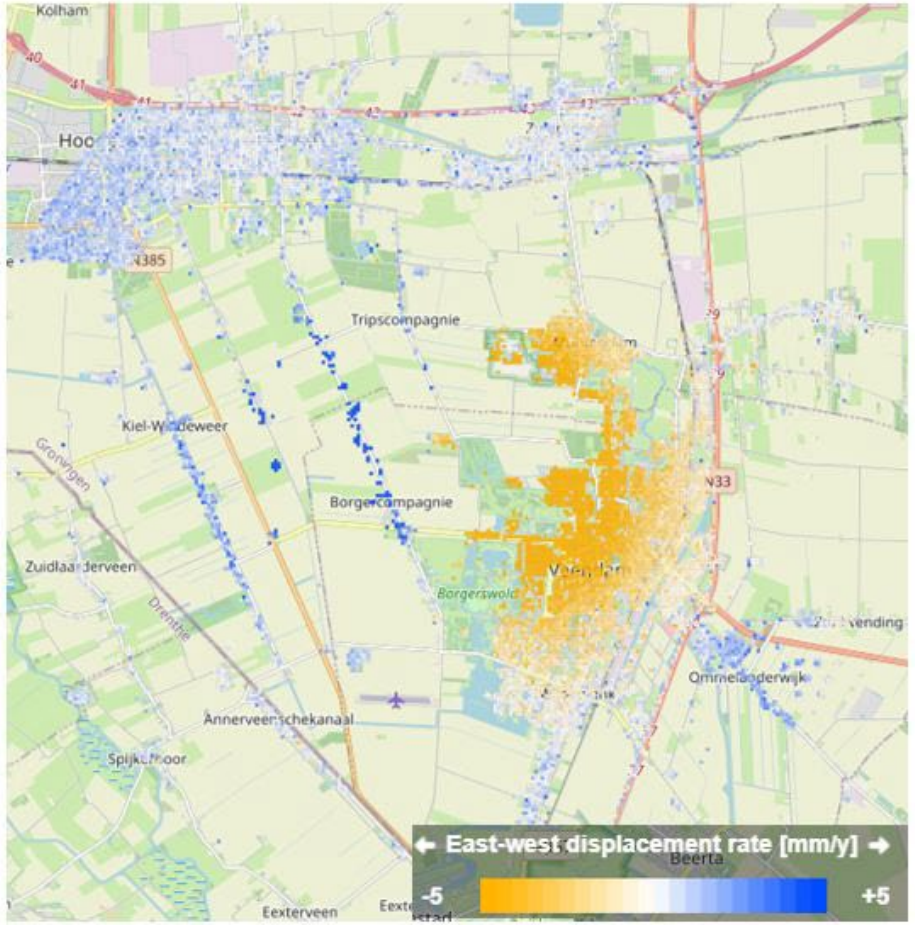
Decomposition error

up-down



A: Vertical displacement rate

east-west



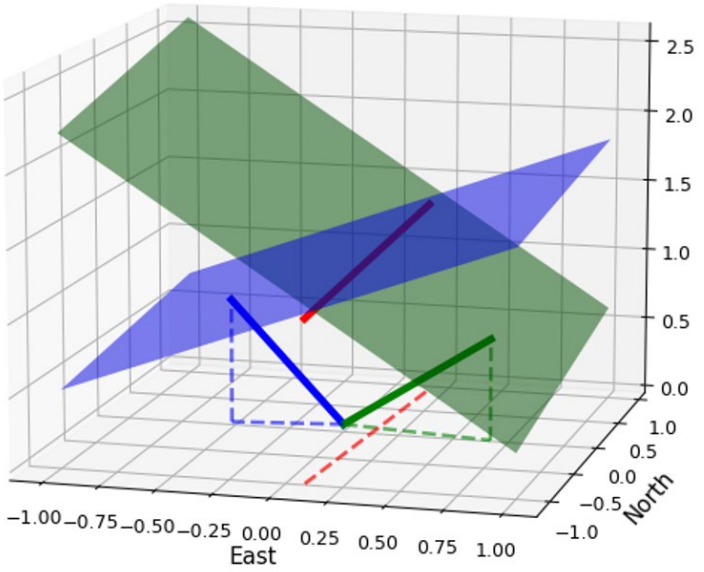
B: East-West displacement rate

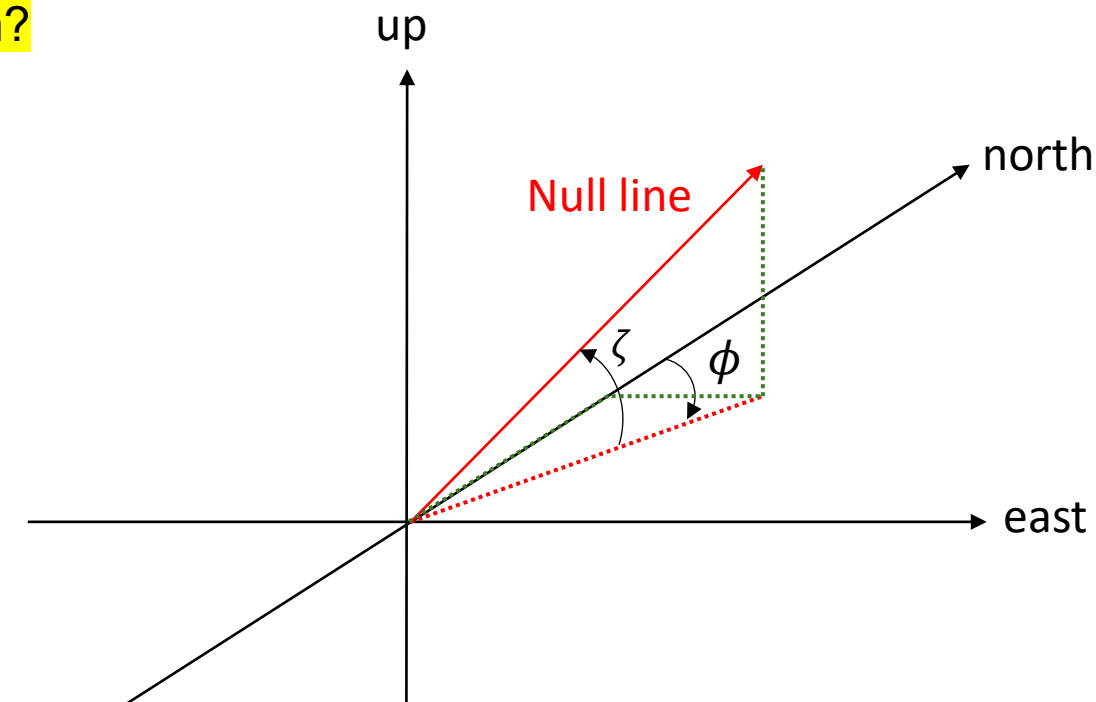
underdetermined problem

$$E\{\underbrace{\begin{bmatrix} d^{\text{asc}}_{\text{LoS}} \\ d^{\text{dsc}}_{\text{LoS}} \end{bmatrix}}_{y}\} = \underbrace{\begin{bmatrix} \sin(\theta_1)\ \sin(\alpha_{d,1}) & \sin(\theta_1)\ \cos(\alpha_{d,1}) & \cos(\theta_1) \\ \sin(\theta_2)\ \sin(\alpha_{d,2}) & \sin(\theta_2)\ \cos(\alpha_{d,2}) & \cos(\theta_2) \end{bmatrix}}_{A} \underbrace{\begin{bmatrix} d_e \\ d_n \\ d_u \end{bmatrix}}_{x}$$

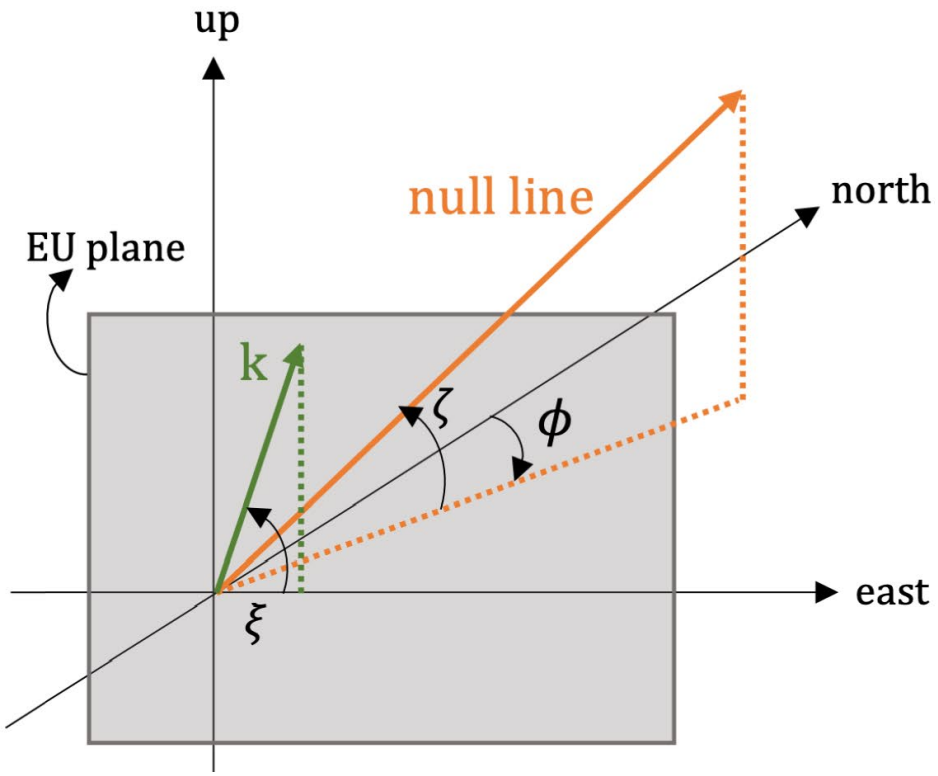
Underdetermined problem: infinite number of solutions, along the "null line"

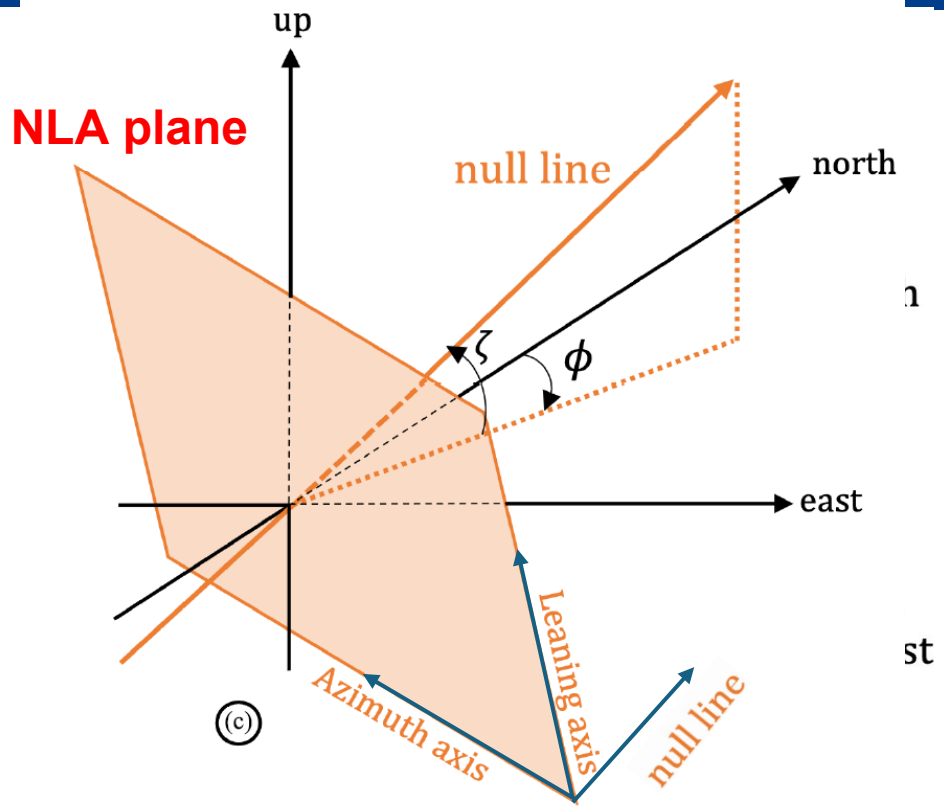
Is there a solution for this problem?





Null-Line Aligned (NLA) reference frame



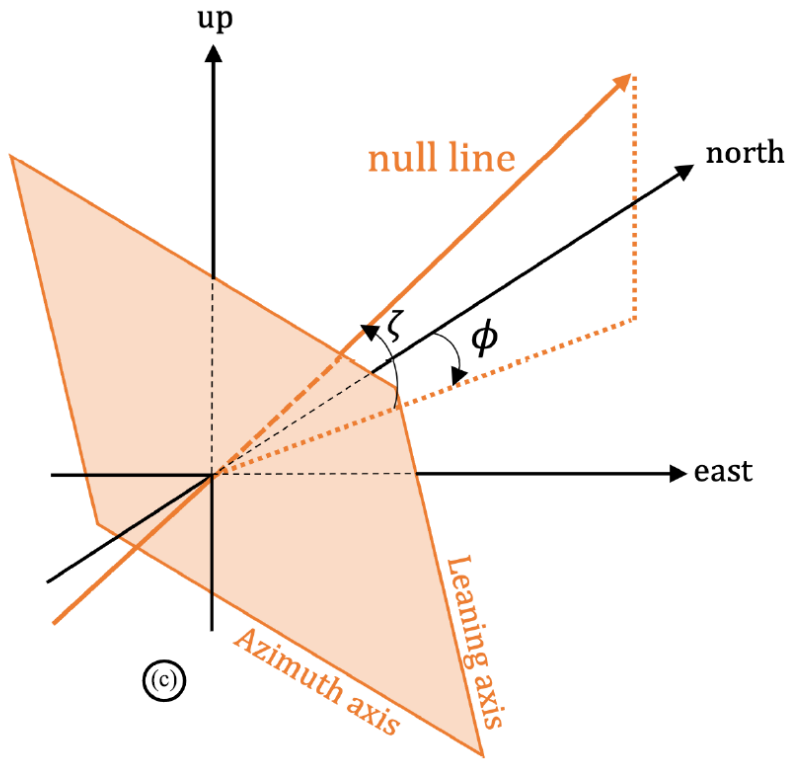


an orthogonal projection of any displacement vector onto the NLA plane will not influence (bias) the two in-plane components.

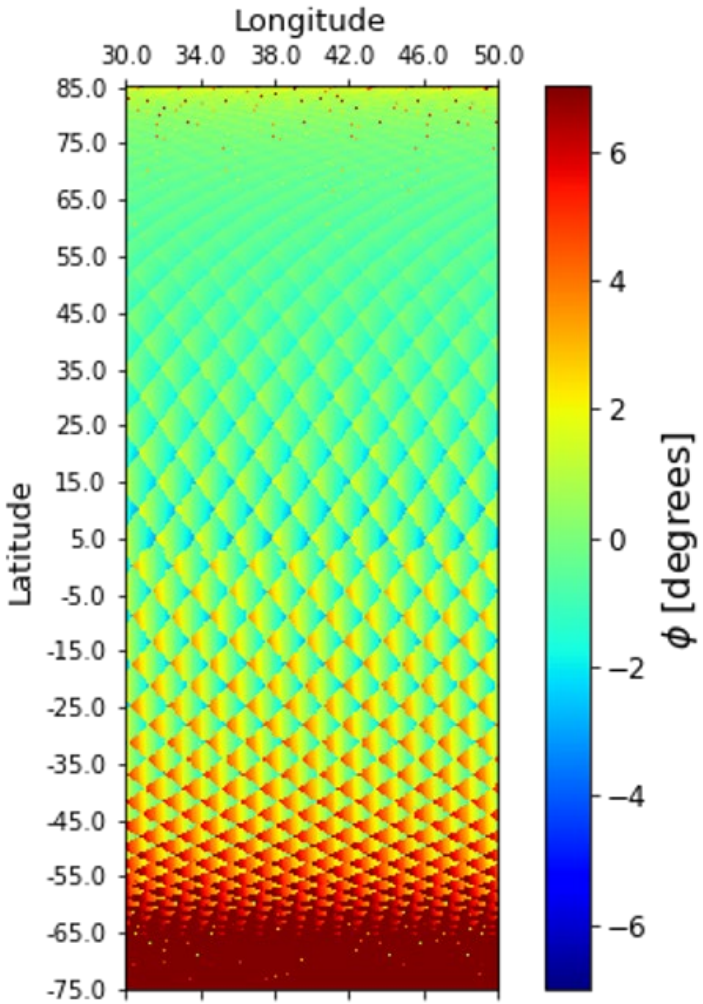
N: null-line (axis), the **L:** leaning axis, tilted backward with elevation angle ζ + 90°, and **A:**azimuth axis, which is horizontal with azimuth ϕ + 90°. Projecting two LoS observation vectors independently onto the NLA plane allows for the simple (and unbiased)retrieval of the resultant vector.

The orientation of the null line (Sentinel-1)

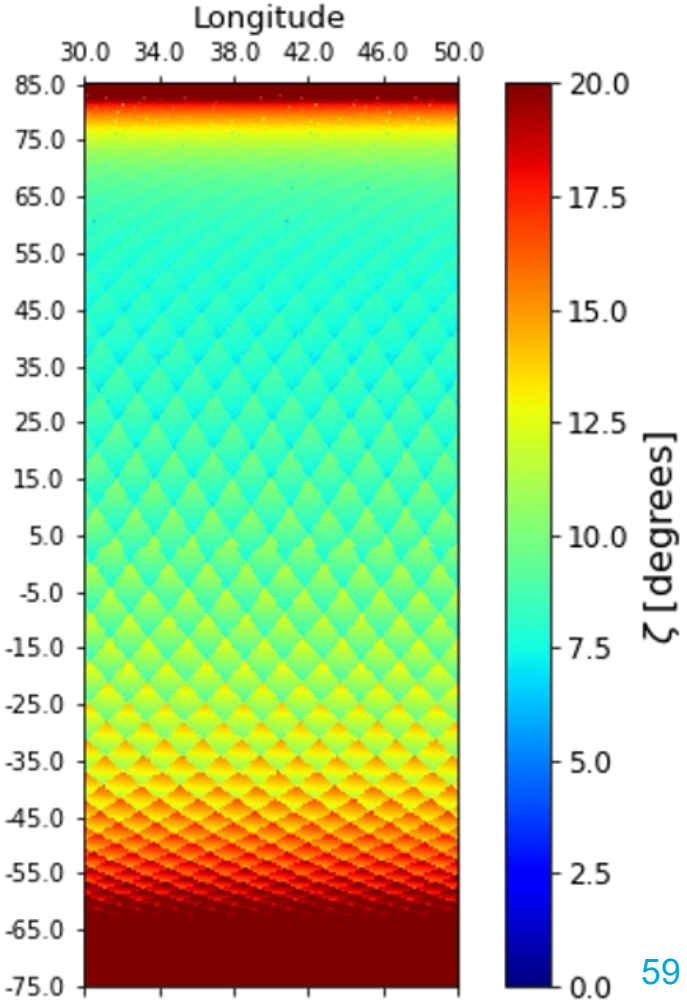
ϕ and ζ are depending on the location on Earth



Azimuth angle



Elevation angle



TU Delft

Download via:
https://gitlab.tudelft.nl/drama/drama

NLA reference frame

- Take home message if we have ascending and descending data:
  - Projecting in the East-Up plane is biased
  - Projecting in the NLA-plan is unbiased

- NLA reference frame:

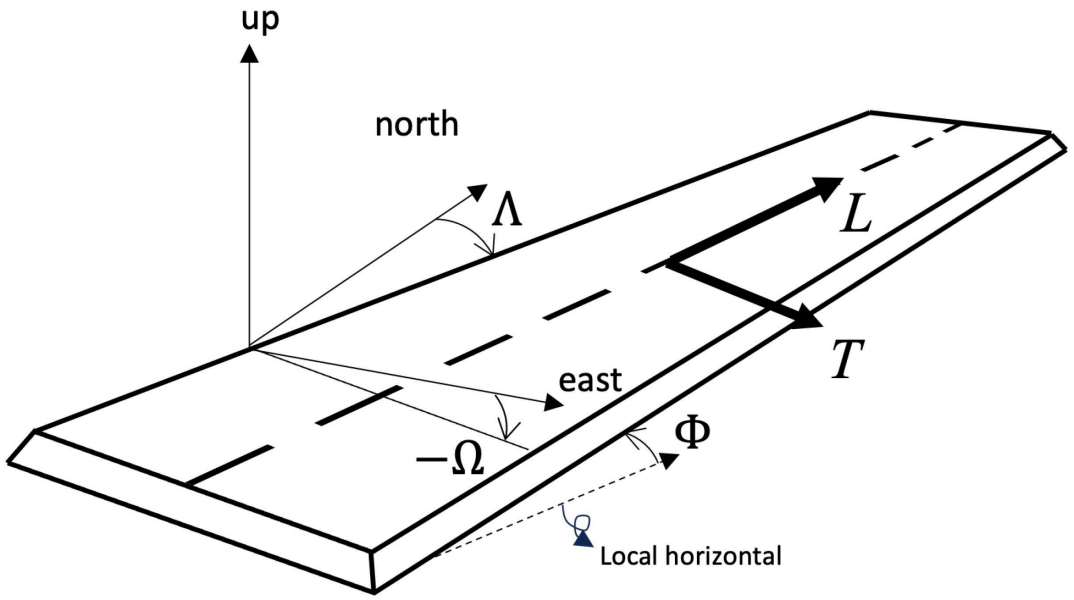
  + unbiased, uniquely interpretable, good for modelling, but less intuitive

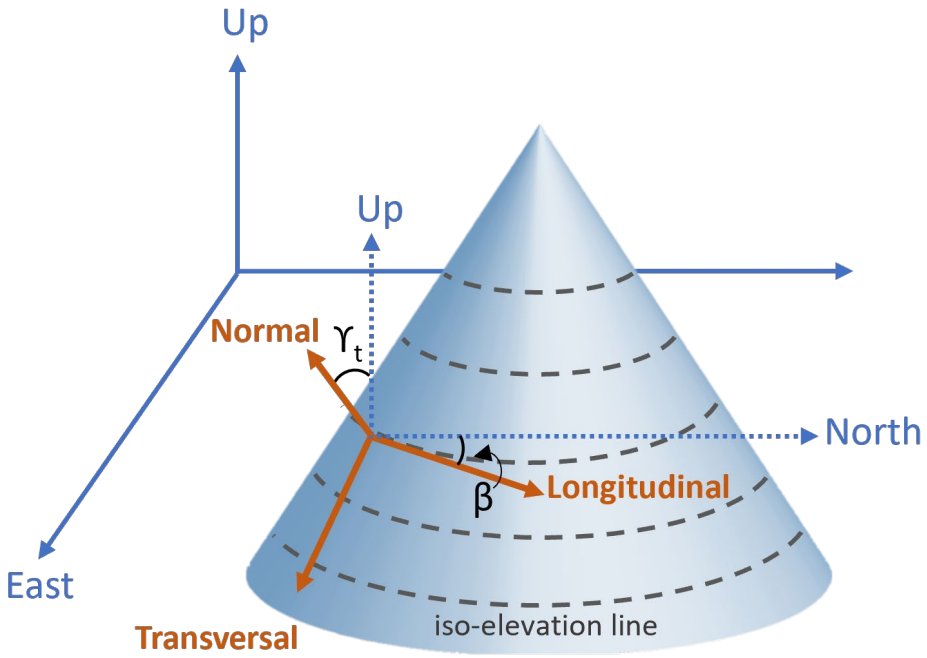
- East-Up: intuitive, but wrong, biased, uninterpretable, bad for modelling

Strap-down approach



- Transversal, Longitudinal, Normal (TLN-frame)
- Orientation: Λ, Ω, Φ
- **Longitudinal displacements are zero**

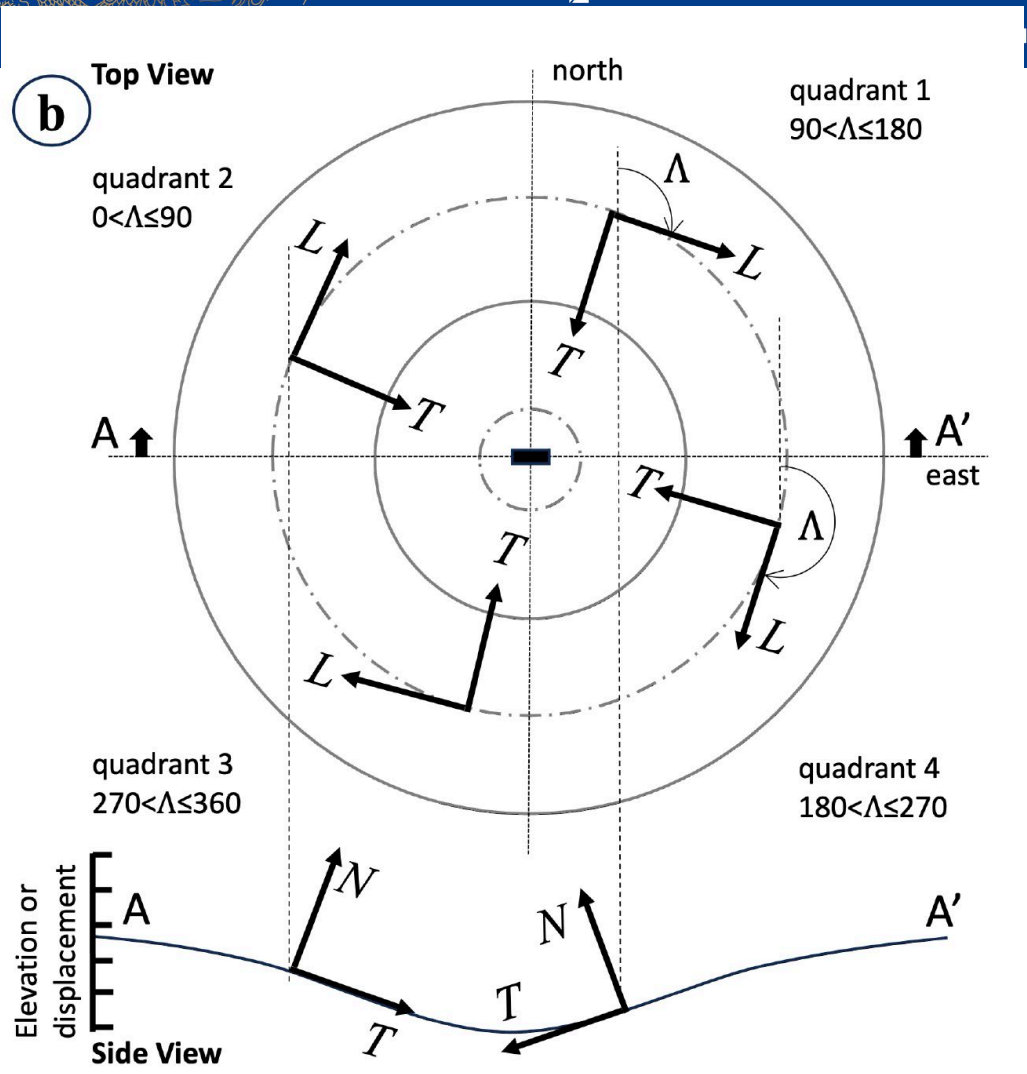




Chang L, Dollevoet RP, Hanssen RF. Monitoring line-infrastructure with multisensor SAR interferometry: Products and performance assessment metrics. IEEE JSTARS. 2018 Mar 2;11(5):1593-605.

Strap-down approach

- Transversal, Longitudinal, Normal (TLN)
- Orientation: Λ, Ω, Φ
- **Longitudinal displacements are zero**



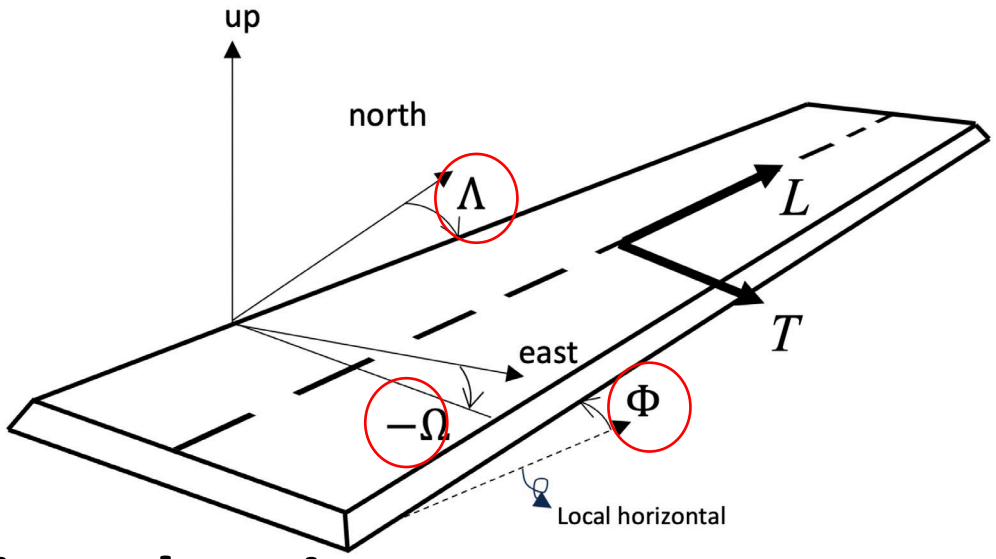
Strap-down approach

- Strap-down coordinate system: Transversal, Longitudinal, Normal

TLN: $$d_{\mathrm{LoS}} = p_{\mathrm{LoS}}\, R_1 R_2 R_3 \begin{bmatrix} d_T \\ \cancel{d_L} \\ d_N \end{bmatrix}$$

$$E\{\underbrace{\begin{bmatrix} d^{(1)}_{\mathrm{LoS}} \\ d^{(2)}_{\mathrm{LoS}} \end{bmatrix}}_{y}\} = \underbrace{\begin{bmatrix} p_{1T} & p_{1N} \\ p_{2T} & p_{2N} \end{bmatrix}}_{A} \underbrace{\begin{bmatrix} d_T \\ d_N \end{bmatrix}}_{x}$$

Orientation of the TLN reference frame



We need to estimate the orientation of the frame → **Biased estimates**

Pseudo observations for frame orientation

Model the uncertainty for the frame alignment

$$E\{\underbrace{\begin{bmatrix} \underline{d}_{\mathrm{LoS}}^{(1)} \\ \vdots \\ \underline{d}_{\mathrm{LoS}}^{(m)} \\ \underline{\Lambda} \\ \underline{\Omega} \\ \underline{\Phi} \end{bmatrix}}_{y}\} = \underbrace{\begin{bmatrix} a_1(x) \\ \vdots \\ a_m(x) \\ a_{m+1}(x) \\ a_{m+2}(x) \\ a_{m+3}(x) \end{bmatrix}}_{A(x)} \underbrace{\begin{bmatrix} p_{1T}d_T + p_{1N}d_N \\ \vdots \\ p_{mT}d_T + p_{mN}d_N \\ \underline{\Lambda} \\ \underline{\Omega} \\ \underline{\Phi} \end{bmatrix}}_{A(x)}$$

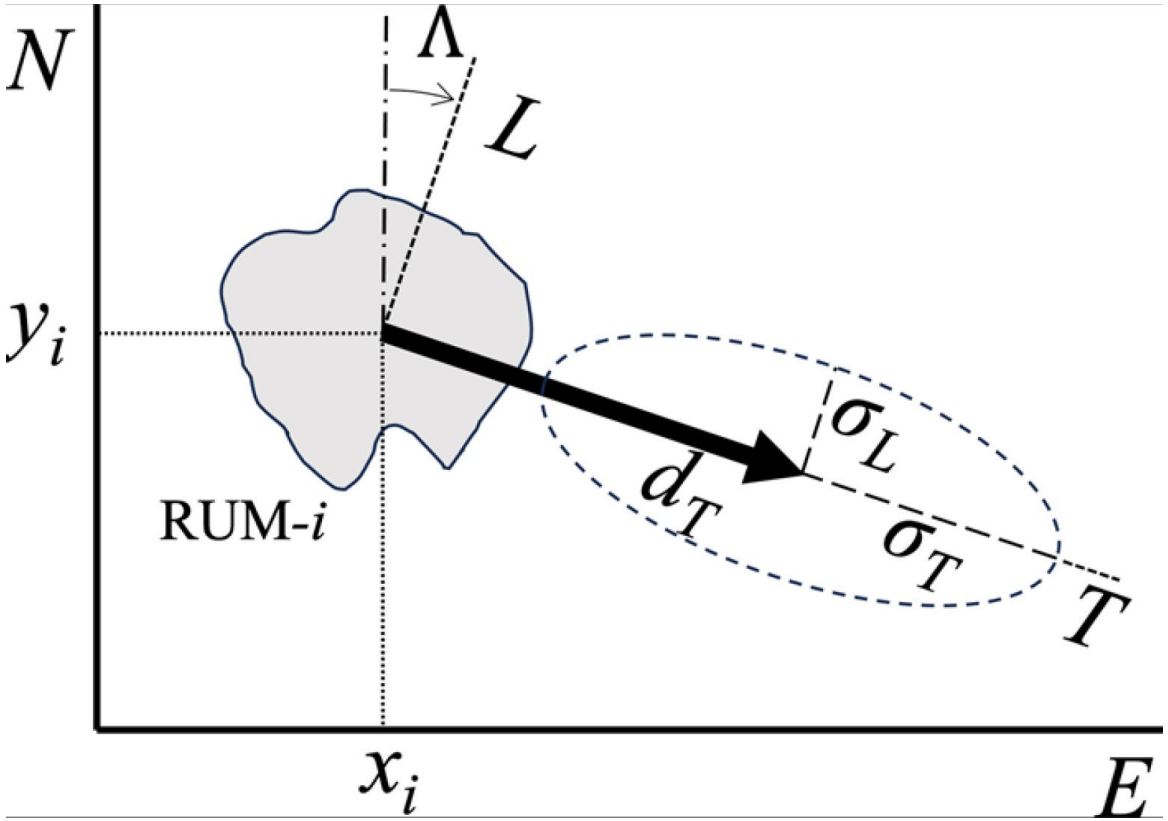
$$D\{\underbrace{\begin{bmatrix} \underline{d}_{\mathrm{LoS}}^{(1)} \\ \vdots \\ \underline{d}_{\mathrm{LoS}}^{(m)} \\ \underline{\Lambda} \\ \underline{\Omega} \\ \underline{\Phi} \end{bmatrix}}_{y}\} = \underbrace{\begin{bmatrix} Q_{\mathrm{LoS},1} & \cdots & 0 & 0 & 0 & 0 \\ \vdots & \ddots & \vdots & 0 & 0 & 0 \\ 0 & \cdots & Q_{\mathrm{LoS},m} & 0 & 0 & 0 \\ 0 & 0 & 0 & \sigma_\Lambda^2 & 0 & 0 \\ 0 & 0 & 0 & 0 & \sigma_\Omega^2 & 0 \\ 0 & 0 & 0 & 0 & 0 & \sigma_\Phi^2 \end{bmatrix}}_{Q_{yy}}$$

Pseudo observations = estimated orientation

'Unknowns'

Uncertainty of the alignment

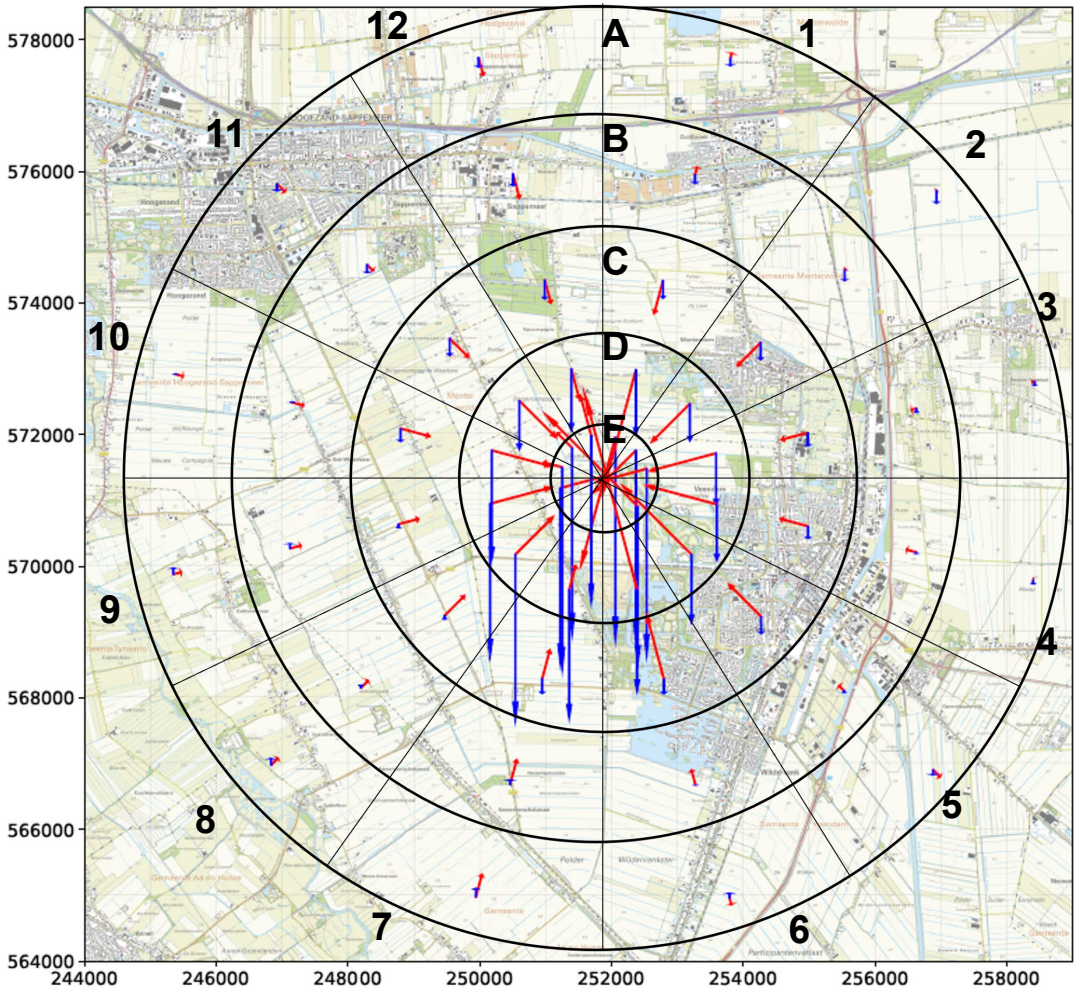
Precision of the strap-down results





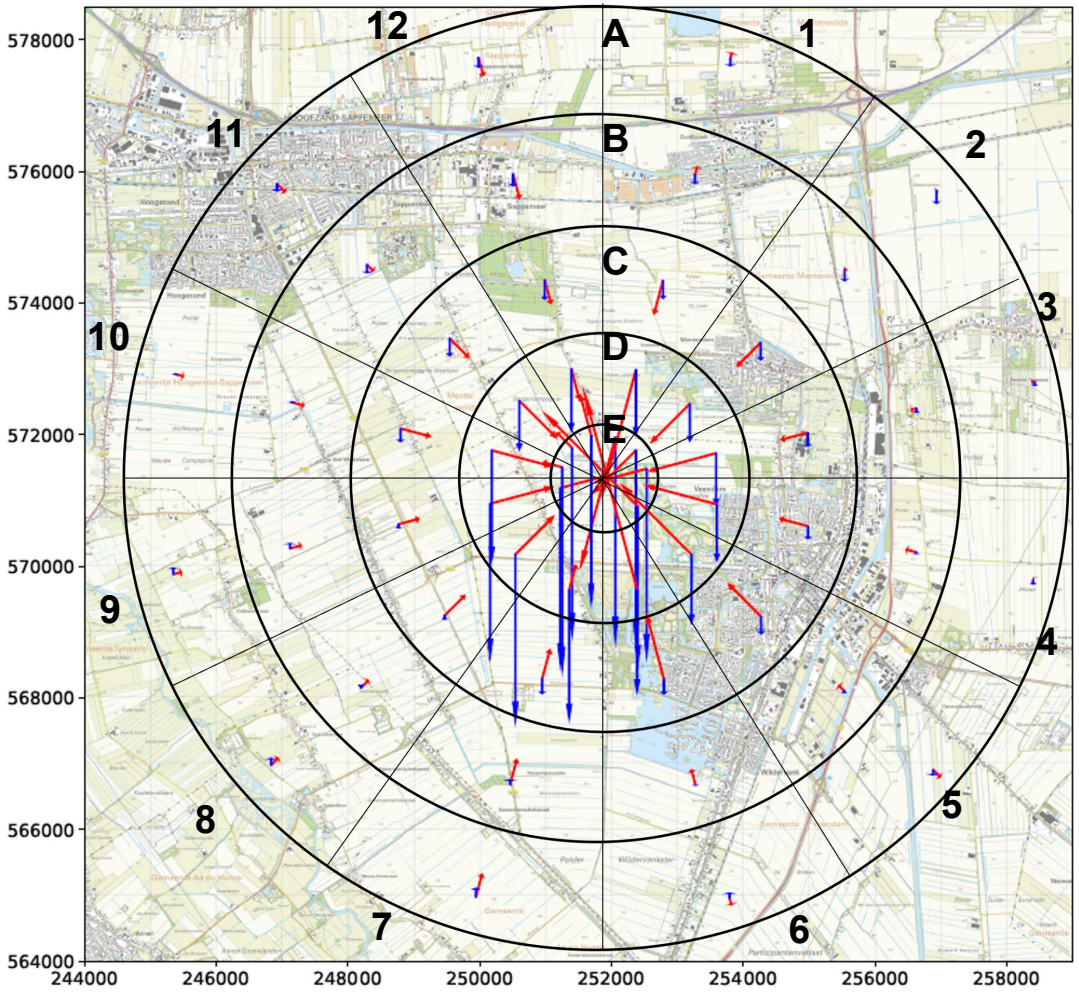
Vector representation of strapdown results of RUM-*i* at geographic (east,north) coordinates (x_i , y_i), showing the estimated transversal displacement component, d_T . The error ellipse or confidence region has two axes. The size of transversal axis is σ_T and the size of the longitudinal axis is $\sigma_L = d_T \tan \sigma_\Lambda$

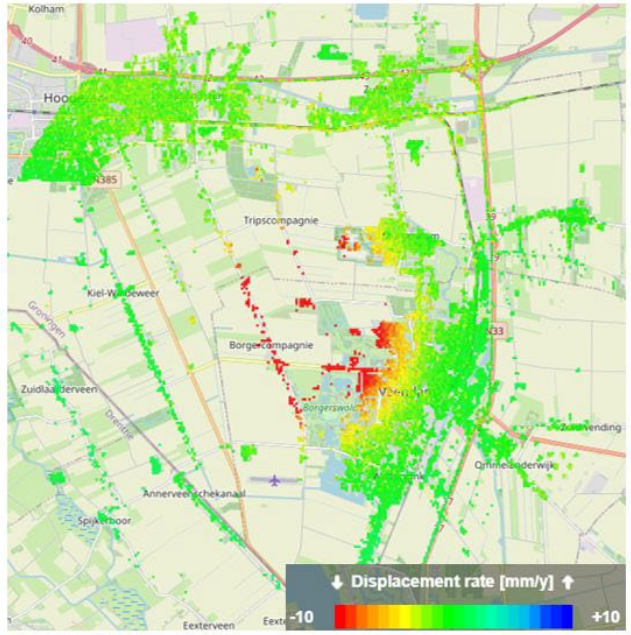
Results: Subsidence bowl



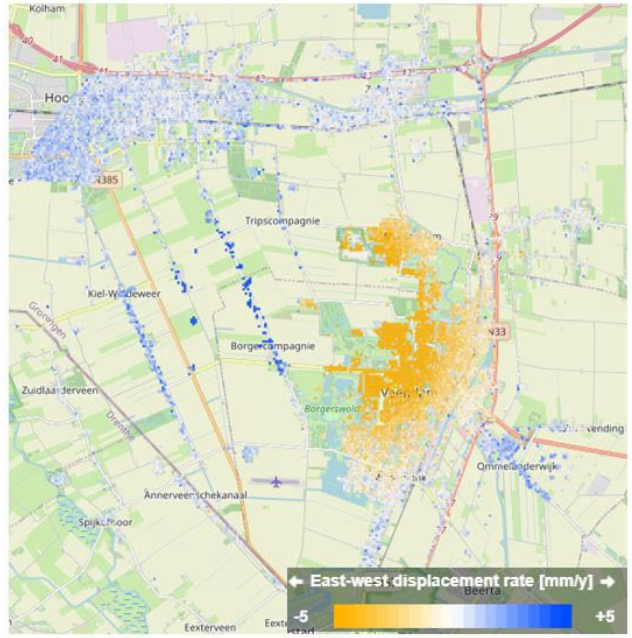
Transversal (near-horizontal, centripetal)
Normal (near-vertical)

Results: Subsidence bowl





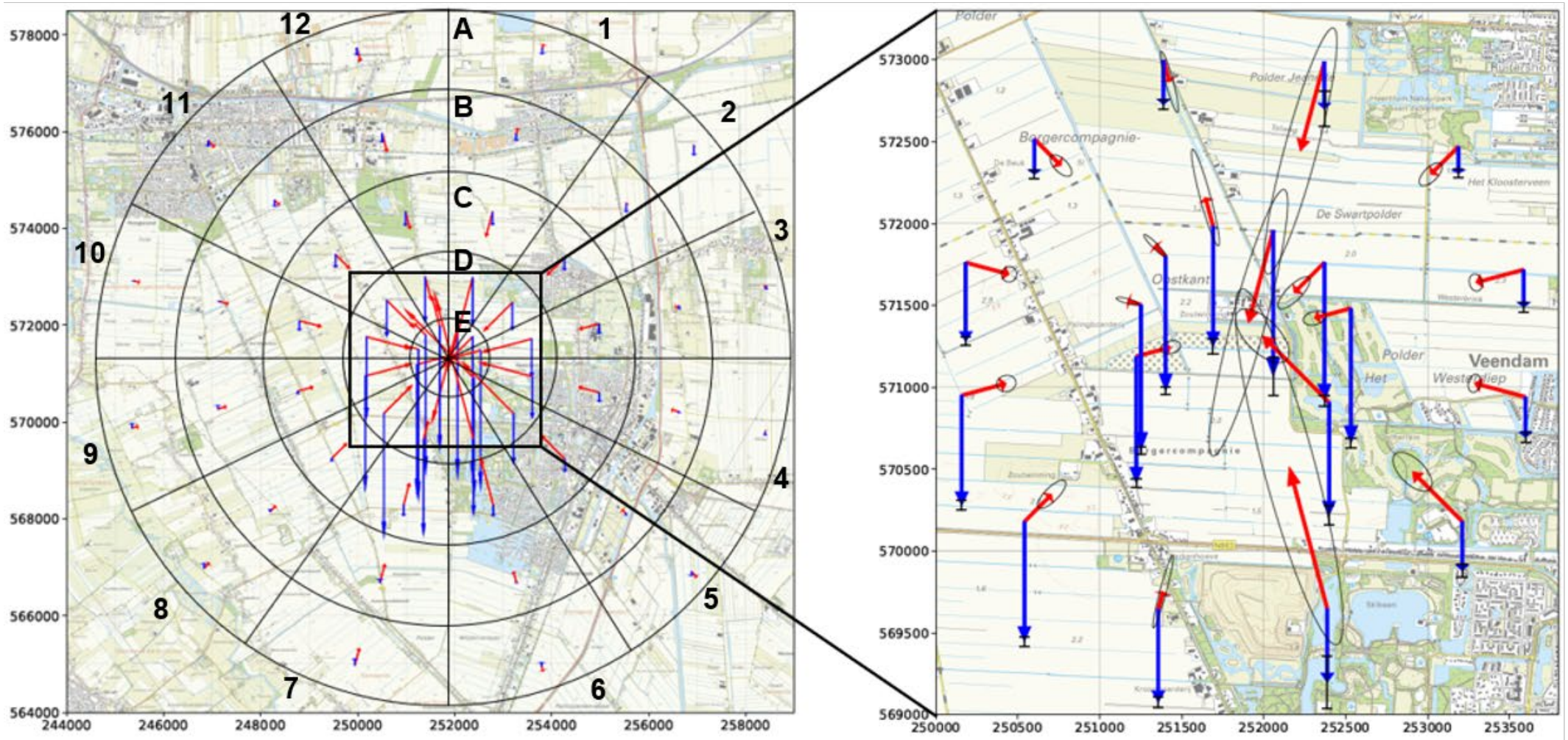
A: Vertical displacement rate



B: East-West displacement rate

Transversal (near-horizontal)
Normal (near-vertical)

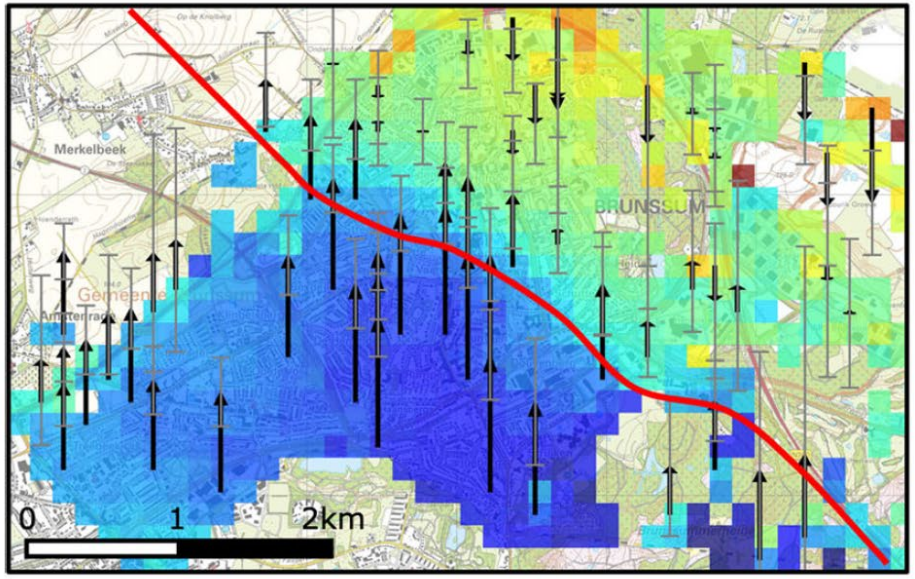
Results: Subsidence bowl – Netherlands



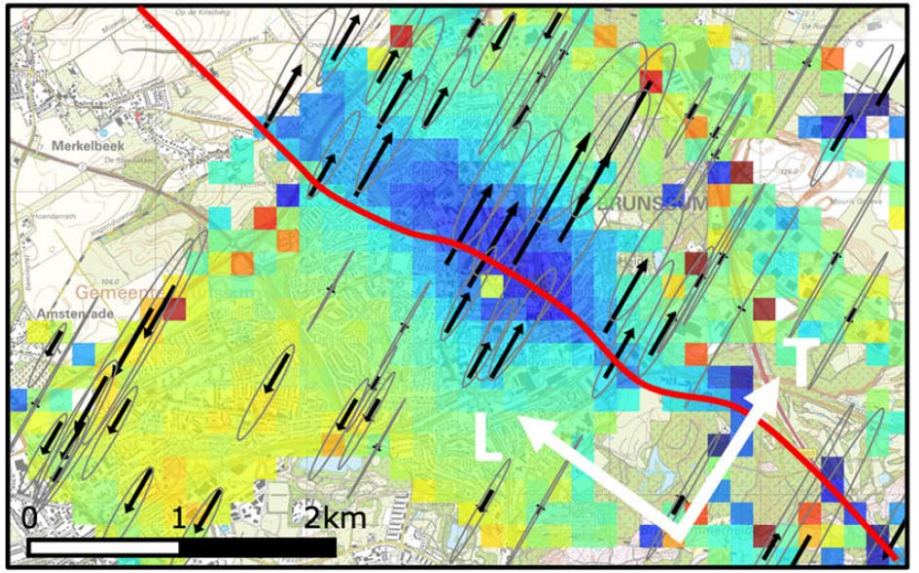
Transversal (near horizontal)

Normal (near vertical)

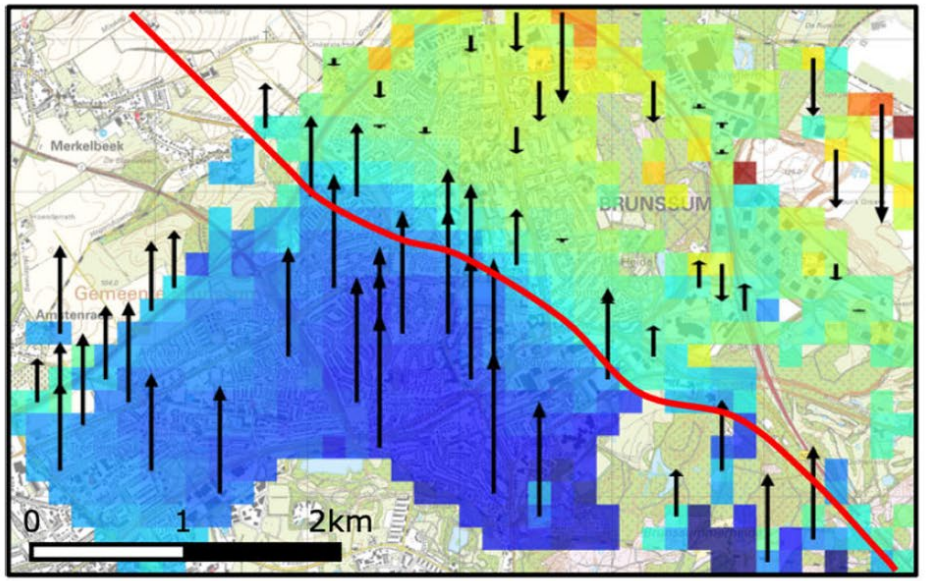
TLN-frame results



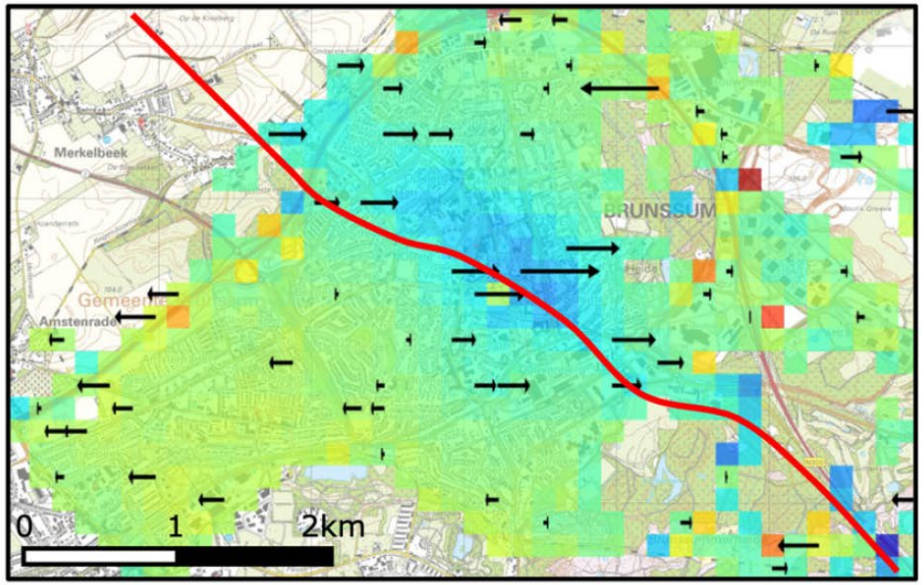
e) Normal



f) Transversal



c) Up



d) East

TU Delft

Conclusions

- InSAR is only sensitive to the projection of the 3D displacements vector onto the Line-of-Sight of the satellite
- With only two satellite observations, this results in an underdetermined problem, with an infinite number of possible solutions along the null-line. The Null-Line Aligned reference frame is unbiased, the East-Up reference frame is biased.
- The strap-down approach is a straightforward physics-based solution to the underdetermination problem resulting in physically more meaningful results, it is 2D-local/ 3D-global
- Traditional geodetic vector-based visualizations with error-ellipses may convey more information than the standard dot-distribution maps used in the InSAR community

Estimating three-dimensional displacements with InSAR: the strapdown approach

Wietske Brouwer[1] · Ramon Hanssen[1]

Received: 8 September 2023 / Accepted: 30 October 2024
© Springer-Verlag GmbH Germany, part of Springer Nature 2024

W. S. Brouwer and R. F. Hanssen, "A Treatise on InSAR Geometry and 3-D Displacement Estimation," in *IEEE Transactions on Geoscience and Remote Sensing*, vol. 61, pp. 1-11, 2023,

